The Astrophysical Journal Supplement Series, 204:3 (25pp), 2013 January doi:10.1088/0067-0049/204/1/3
© 2013. The American Astronomical Society. All rights reserved. Printed in the U.S.A.

YONSEI EVOLUTIONARY POPULATION SYNTHESIS (YEPS) MODEL. I. SPECTROSCOPIC EVOLUTION OF SIMPLE STELLAR POPULATIONS

Chul Chung[1], Suk-Jin Yoon[1], Sang-Yoon Lee, and Young-Wook Lee
Department of Astronomy & Center for Galaxy Evolution Research, Yonsei University, Seoul 120-749, Republic of Korea; ywlee2@yonsei.ac.kr
Received 2012 August 20; accepted 2012 October 19; published 2012 December 14

ABSTRACT

We present a series of papers on the 2012 version of the Yonsei Evolutionary Population Synthesis (YEPS) model, which was constructed based on over 20 years of research. This first paper delineates the spectroscopic aspect of integrated light from stellar populations older than 1 Gyr. The standard YEPS is based on the most up-to-date Yonsei–Yale stellar evolutionary tracks and BaSel 3.1 flux libraries, and provides absorption line indices of the Lick/IDS system and high-order Balmer lines for simple stellar populations as functions of stellar parameters, such as metallicity, age, and α-element mixture. Special care has been taken to incorporate a systematic contribution from horizontal-branch (HB) stars, which alters the temperature-sensitive Balmer lines significantly, resulting in up to a 5 Gyr difference in the age estimation of old, metal-poor stellar populations. We also find that HBs exert an appreciable effect not only on the Balmer lines but also on the metallicity-sensitive lines, including the magnesium index. This is critical in explaining the intriguing bimodality found in index distributions of globular clusters in massive galaxies and to accurately derive spectroscopic metallicities from various indices. A full set of the spectroscopic and photometric YEPS model data of the entire parameter space is currently downloadable at http://web.yonsei.ac.kr/cosmic/data/YEPS.htm.

Key words: globular clusters: general – stars: abundances – stars: evolution – stars: general – stars: horizontal-branch

1. INTRODUCTION

The Evolutionary Population Synthesis (EPS) technique is a key tool for interpreting integrated light from remote stellar systems. Based on stellar evolution theories, the EPS models place constraints on ages, chemical abundances, and star formation histories of star clusters and galaxies (e.g., Tinsley 1978; Bruzual 1983; Arimoto & Yoshii 1987; Guiderdoni 1987; Buzzoni 1989; Bruzual & Charlot 1993; Bressan et al. 1994; Fritze-Von Alvensleben & Gerhard 1994; Worthey 1994a; Letherer 1995; Park & Lee 1997; Yi et al. 1997; Fioc & Rocca-Volmerange 1997; Maraston 1998; Vazdekis 1999; Schulz et al. 2002; Thomas et al. 2003; Bruzual & Charlot 2003; Lee et al. 2005a; Lee & Worthey 2005; Schiavon 2007; Cervantes & Vazdekis 2009; Lee et al. 2010; Vazdekis et al. 2010; Conroy & Gunn 2010; Percival & Salaris 2011; Maraston & Strömbäck 2011; Pforr et al. 2012). Combined with recent developments in high precision observations, the EPS models are becoming more important for the analyses of various stellar populations in galaxies.

In a series of papers, we intend to present the Yonsei Evolutionary Population Synthesis (YEPS) model for the spectroscopic and photometric evolution of simple stellar populations (SSPs). This paper, as the first paper of the series, describes the spectroscopic aspect of our YEPS model. The model is constructed by the YEPS Fortran code package, which has been improved and exploited for the past 20 years by many studies related to (1) synthetic color–magnitude diagrams (CMDs) for individual stars (e.g., Lee et al. 1990, 1994, 2005a; Rey et al. 2001; Yoon & Lee 2002; Kim et al. 2006; Yoon et al. 2008; Han et al. 2009) and (2) synthetic integrated spectra for colors and absorption indices of simple and composite stellar populations (e.g., Park & Lee 1997; Lee et al. 2000, 2005b; Rey et al. 2005, 2007, 2009; Kaviraj et al. 2005, 2007a, 2007b, 2007c; Ree et al. 2007; Yoon et al. 2006, 2009; Yoon & Chung 2009; Spitler et al. 2008; Mieske et al. 2008; Choi et al. 2009; Chung et al. 2011; Yoon et al. 2011b, 2011a; Cho et al. 2012). The forthcoming Paper II (S.-J. Yoon et al. 2013, in preparation) will present the photometric evolution of stellar populations. Future papers in the series will discuss the effects of the different choices of ingredients and input parameters on the model, as well as the application of YEPS for early-type galaxies that have composite stellar populations.

The standard YEPS model has been constructed based on the Yonsei–Yale (Y^2) stellar evolution models (Kim et al. 2002; Y.-W. Lee et al. 2013, in preparation) and the BaSeL flux library (Westera et al. 2002). The absorption-line index model employs the Lick/IDS system (Burstein et al. 1984; Faber et al. 1985; Worthey 1994a; Worthey & Ottaviani 1997; Schiavon 2007), which defines 25 absorption lines produced by various elements at the surface of the stellar atmosphere. The Lick/IDS system uses the spectra of nearly 460 stars to cover a wide parameter space of temperature, gravity, and metallicity (Buzzoni et al. 1992, 1994; Worthey 1994a; Worthey & Ottaviani 1997; Schiavon 2007). The system, however, does not consider the α-element enhancement grid, and thus the enhancement should be treated theoretically. We applied the α-element correction terms by Korn et al. (2005) to our model, following the schemes used by Trager et al. (2000), Thomas et al. (2003), and Schiavon (2007).

The YEPS model has been built with particular interest in dealing with the core helium-burning horizontal-branch (HB) stars. Since the presence of hot stars in globular clusters (GCs) and galaxies changes the overall shape and absorption features of their spectral energy distributions (SEDs), especially at short wavelengths, the impact of hot HB stars ($\gtrsim$8000 K) has been a topic of great interest in the EPS community over the past 20 years (Lee et al. 1990, 1994; Worthey 1994b; Lee et al. 2000; Thomas et al. 2003; Lee et al. 2005a; Schiavon 2007; Yoon et al. 2006, 2008, 2011a, 2011b, 2012). Lee et al. (2000) first

[1] Both authors have contributed equally to this paper.

Table 1
Model Input Parameters

Input Ingredients and Parameters	Standard Model	Comparison Model
Stellar library	Y^2 stellar libraries	BaSTI
	(Kim et al. 2002; Y.-W. Lee et al. 2013 in preparation)	(Pietrinferni et al. 2004)
Spectral library	BaSel 3.1 (Westera et al. 2002)	BaSel 3.1 (Westera et al. 2002)
Empirical fitting functions	Worthey (1994a)	Worthey (1994a)
	Worthey & Ottaviani (1997)	Worthey & Ottaviani (1997)
	Schiavon (2007)	Schiavon (2007)
Response functions of α-elements	Korn et al. (2005)	Korn et al. (2005)
Initial mass function	Salpeter ($x = 1.35$)	Salpeter ($x = 1.35$)
α-element enhancement, [α/Fe]	0.0, 0.3, 0.6	0.0, 0.4
HB mass dispersion, $\sigma_M(M_\odot)$	0.015	0.015
Reimers (1977)'s mass-loss efficiency parameter, η	0.63	0.40[a]
Assumption of the age of inner-halo MWGCs	12 Gyr	12 Gyr

Note. [a] For our models with the BaSTI stellar library, we have applied the additional mass loss of 0.01 $M_\odot$ in order to reproduce HB morphologies of inner halo GCs in the MW at the age of 12 Gyr.

demonstrated that the Hβ absorption index—the most popular age indicator—is significantly enhanced by the presence of blue HB stars. More recently, Yoon et al. (2006, 2011a, 2011b) showed that the systematic metallicity-dependent variation in the HB temperature leads to the nonlinear relationship between metallicity and broadband optical colors. Despite the fact that hot, blue HB stars exert a strong effect on properties of integrated light from GCs and galaxies, most EPS models to date take into account the details of HBs in a fairly limited manner. YEPS, by contrast, defines the HB effect not merely as a contamination factor, but as a crucial part of the EPS model for various spectroscopic and photometric observables.

The paper is organized as follows. Section 2 describes the procedure for constructing the YEPS model. Section 3 presents the results of our stellar population simulations and the comparison of our model with observations. Section 4 discusses the implications, and, finally, Section 5 summarizes our results. A full set of the spectroscopic and photometric YEPS model data of the entire parameter space is available at http://web.yonsei.ac.kr/cosmic/data/YEPS.htm.

2. CONSTRUCTION OF THE YEPS MODEL

For a given stellar system, the YEPS model provides (1) synthetic CMDs (Section 2.1), (2) synthetic SEDs (Section 2.2), (3) the integrated absorption line indices (Section 2.3), (4) the integrated magnitudes and broadband colors, and (5) the integrated surface brightness fluctuations. Table 1 summarizes the ingredients and input parameters of the YEPS model.

2.1. Synthetic Color–Magnitude Diagrams

The standard YEPS model is constructed based on the most up-to-date Yonsei–Yale (Y^2) stellar evolutionary tracks. For the evolutionary phases from the main sequence (MS) to the tip of the red giant branch (RGB), we used Y^2-isochrones (Kim et al. 2002; Y.-W. Lee et al. 2013, in preparation), covering the metallicity grids from $Z = 0.00001$ to 0.08 with three different values for the α-element enhancement ([α/Fe] = 0.0, 0.3, and 0.6). The mixture pattern of the α-element enhancement in Y^2-isochrones follows that of VandenBerg et al. (2000). The Y^2 stellar evolutionary libraries adopt a galactic helium enrichment parameter of $\Delta Y/\Delta Z = 2.0$ with a primordial helium abundance of $Y = 0.23$. To examine the effect of the different choice of evolutionary tracks, we comparatively used the BaSTI stellar evolutionary tracks (Pietrinferni et al. 2004) with metallicities from $Z = 0.0001$ to 0.04 for the two α-element enhancement cases ([α/Fe] = 0.0 and 0.4). The Y^2 stellar libraries include helium diffusion, and the BaSTI stellar libraries include the atomic diffusion of both helium and metals. As will be demonstrated below, the major features of our model do not depend on the specific choice of stellar libraries.

We adopt the Salpeter initial mass function (IMF) for our standard set of simulations in order to assign the number of stars along given isochrones. Worthey (1994a) presented the generalized Salpeter IMF of the form:

$$\frac{dN}{dM} = \frac{M_{\rm tot}(1-x)}{M_u^{1-x} - M_l^{1-x}} M^{-(1+x)}, \qquad (1)$$

where dN is the number of stars within the fixed mass bin dM, and M_l and M_u are the lower and upper mass cuts, respectively. From this, we calculated the IMF of an SSP that consists of a single-metallicity and a single-age population. We have applied 10^6 stars within the whole mass range of the IMF (from 0.2 to 5.0 $M_\odot$). We adopted the standard Salpeter index ($x = 1.35$) over the whole mass range. The choice of x exerts a fairly small effect on the overall shape of UV-to-IR SEDs and thus on broadband colors and absorption indices (Park & Lee 1997). This applies even more for old stellar populations for which massive stars have already evolved off the MS, because the index x controls the fractional contribution from the massive stars. However, it is noteworthy that x leads to significant variations in the total absolute magnitude of the model SSPs (Tinsley 1972), because the absolute flux level of SEDs is a function of the total stellar mass.

For the synthetic HB modeling, we used Y^2-HB tracks (Y.-W. Lee et al. 2013, in preparation) that are fully consistent with Y^2-isochrones in terms of the input physics and assumed parameters. The Y^2-HB tracks cover a wide range of the HB total mass, from 0.4438 $M_\odot$ for $Z = 0.06$ and 0.5037 $M_\odot$ for $Z = 0.0001$ to 1.5 $M_\odot$ for all metallicities, to incorporate the wide variation of HB morphology. In order to simulate the mass dispersion of HB stars, we used the Gaussian HB mass distribution of the form

$$P(M) \propto \exp\left(\frac{-(M - \langle M_{\rm HB}\rangle)^2}{2\sigma_M^2}\right), \qquad (2)$$

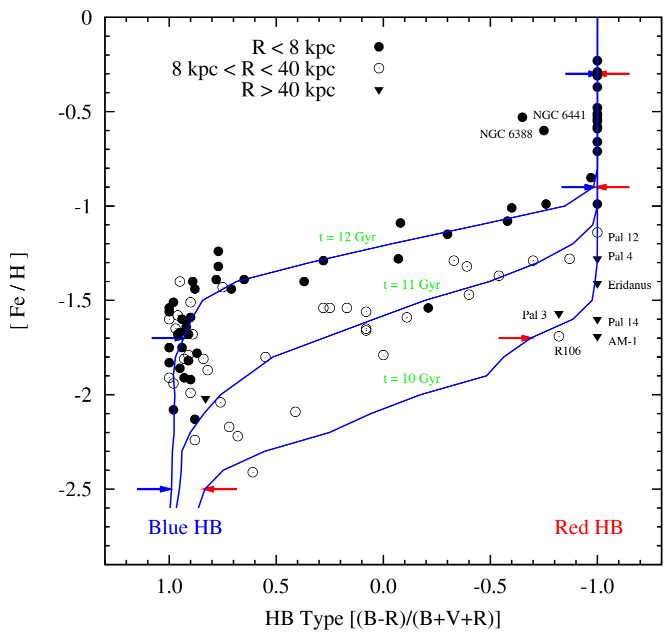

Figure 1. Variation of HB morphology as functions of metallicity and age. The filled and open circles and triangles are GCs in three radial zones of the Milky Way (Lee et al. 1994, 2007). The solid blue lines are theoretical isochrones from the 10, 11, and 12 Gyr YEPS model. The blue and red arrows indicate the selected metallicities ([Fe/H] = −2.5, −1.7, −0.9, and −0.3) for the synthetic color–magnitude diagrams (CMDs) in Figure 2.

where $P(M)$ is the probability density function of the HB mass, and $\langle M_{\rm HB}\rangle$ is the mean mass of the HB at a given metallicity and age. The standard model assumed the value of σ_M to be $0.015\,M_\odot$ (Lee et al. 1990, 1994). On average, the number of HB stars at a given metallicity and age is 350 in a single simulation. In addition, in order to avoid small number statistics in HB modeling, we repeated the simulation 10 times to get the averaged continuum flux at a given metallicity and age.

Figure 1 shows how the HB morphology of the YEPS model[2] is calibrated to the observations. The HB type is defined as $(B - R)/(B + V + R)$, where B, R, and V are the numbers of blue and red HB stars and RR Lyrae variable stars, respectively (Lee et al. 1994). Filled circles represent the oldest inner-halo ($R_{\rm GC} < 8$ kpc) Milky Way globular clusters (MWGCs), and open circles ($8 < R_{\rm GC} < 40$ kpc) and triangles ($R_{\rm GC} > 40$ kpc) represent the outer-halo MWGCs. Solid lines from top to bottom are the HB-type variation of the YEPS model with varying ages. The free parameter, the Reimers mass-loss efficiency parameter η, is used to calibrate our model HB types to the observations. We adopted Reimers' (1977) empirical formula for the mass loss along the RGB (Rood 1973; Lee et al. 1990). The formula takes the form of $dM/dt \propto \eta(L/gR)$, where L, g, and R are the luminosity, gravity, and radius of stars, respectively. The comparison of models and observations suggests an η of 0.63 under the assumption that the mean age of inner-halo GCs is 12 Gyr (Gratton et al. 1997; Reid 1997; Chaboyer et al. 1998; Marín-Franch et al. 2009; Dotter et al. 2010). Figure 2 shows the CMDs for selected model SSPs (red and blue arrows in Figure 1). In general, the HB type becomes redder with increasing metallicity and decreasing age (e.g., Lee et al. 1994).

[2] Recent observations and modeling indicate that an abundance anomaly, especially in He and CNONa, is present in the MWGCs with multiple stellar populations. Although the variation in the He and the CNONa abundance among GCs in the MW is large, the average variation between GC systems in different galaxies, as a whole, is not expected to vary greatly. Additionally, only 30% of the MWGCs are significantly affected by the enhancement in He (Lee et al. 2007), and this suggests that HB morphologies in the majority of the MWGCs are mostly controlled by total metallicity and age. However, if the average He enhancement in the MWGCs is not archetypical and it varies significantly from one galaxy to another, our models presented here would need further revisions to reflect this.

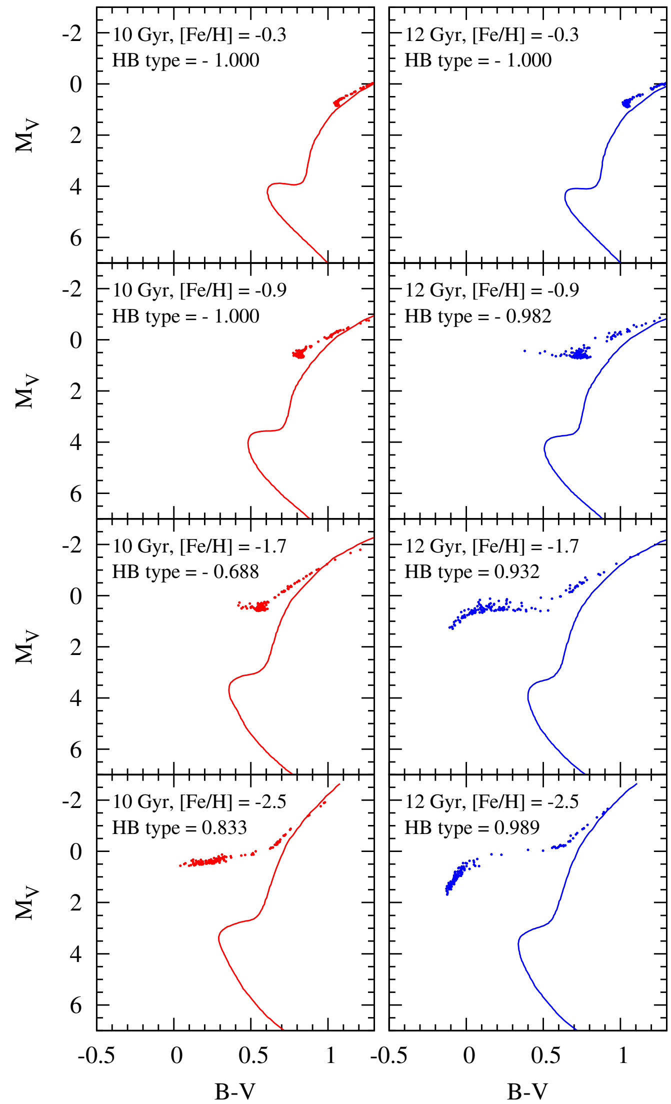

Figure 2. Effect of metallicity and age on the morphology of HB stars in the CMD. The metallicity of each CMD increases from the bottom to the top panels. CMDs on the left and right sides are 10 and 12 Gyr models, respectively. The solid lines are isochrones, and the dots are the corresponding HB stars at given ages and metallicities.

2.2. *Synthetic Spectral Energy Distributions*

SEDs of SSPs are generated based on the synthetic CMDs (Section 2.1). The CMDs give stellar parameters of individual stars in given SSPs, including effective temperature (T), surface gravity (g), global metallicity ([Z/H]), and α-element enhancement ([α/Fe]). To derive theoretical spectral fluxes (in units of [erg s^{-1} cm^{-2} Å]), we use the spectral library of BaSel 3.1 (Westera et al. 2002). BaSel 3.1 is based on the expertise of Kurucz (1992) and BaSel 2.2 (Lejeune et al. 1998), and provides extensive and homogeneous grids of theoretical flux distributions calibrated to the colors of the MWGCs at all levels of metallicity. The library covers effective temperatures from 2000 K to 50,000 K, gravities in a solar unit from $\log g$ of

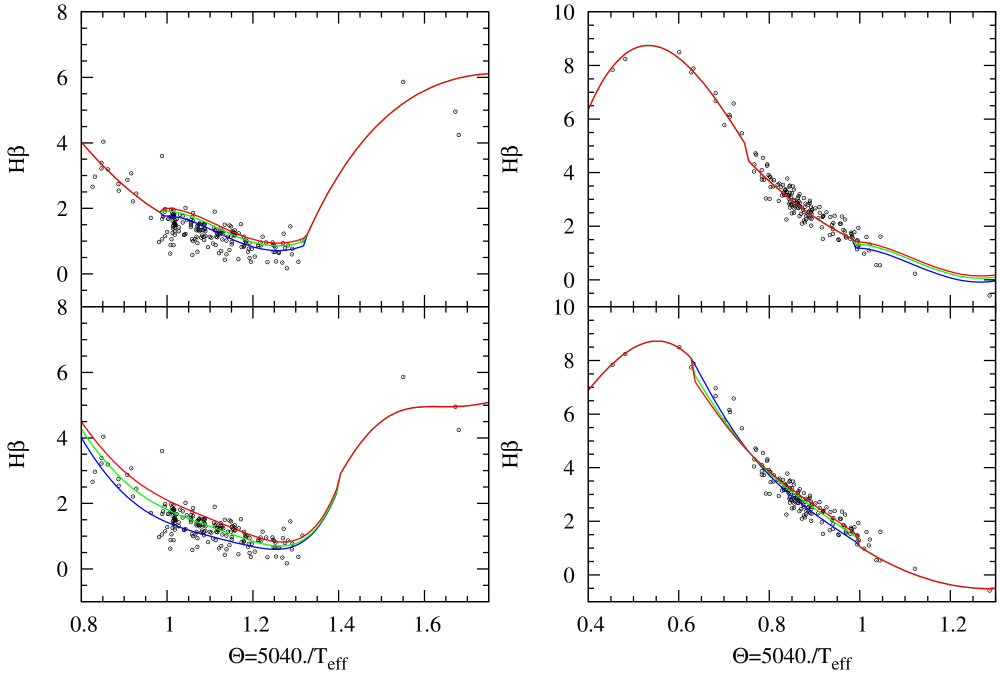

Figure 3. Hβ fitting functions with respect to gravity and temperature ($\Theta = 5040/T_{\rm eff}$). The black dots are H$\beta$ measurements of 460 stellar spectra used for the construction of W94's fitting functions. The left panels are fitting functions for giant stars (with $\log g \leqslant 3.6$) and the right panels are fitting functions for dwarf stars (with $\log g \geqslant 3.6$). The upper and lower panels are fitting functions of W94 and S07, respectively. The red, green, and blue solid lines indicate metallicities of [Fe/H] = −1.0, −0.3, and 0.1, respectively.

−1.02 to 5.50, and metallicities [Z/H] from −2.0 to 0.5. Note that the BaSel 3.1 library assumes scaled-solar α-elements. We thus choose to use the total metallicity [Z/H] for the construction of SEDs of SSPs, rather than the iron abundance [Fe/H].[3] The equation $[Z/H] = [Fe/H] + A\,[\alpha/Fe]$ relates [Z/H] to [Fe/H]. In our model for $[\alpha/Fe] = 0.3$, the factor A, which depends on the α-element mixture of the model, equals 0.723.

We calculate the expected flux F_λ at a distance d using the form

$$F_\lambda = 4\pi \times \frac{L}{\sigma T_{\rm eff}^4} \times H_\lambda \times \frac{1}{4\pi d^2}, \tag{3}$$

where H_λ, L, $T_{\rm eff}$, and σ are the flux intensity, the luminosity, the effective temperature of a star, and the Stefan–Boltzmann constant, respectively. From these fluxes of individual stars, integrated fluxes of all stages of stellar populations in the synthetic CMDs—MS to RGB, HB, and post-asymptotic giant branch (PAGB)—are calculated using the following summation form:

$$F_\lambda^{\rm total} = F_\lambda^{\rm MS} + F_\lambda^{\rm RGB} + F_\lambda^{\rm HB} + F_\lambda^{\rm PAGB}. \tag{4}$$

The total mass of SSPs at a given age and metallicity is normalized to $10^6\,M_\odot$.

2.3. Absorption-line Strength Indices

The absorption-line indices of the YEPS model are calculated using the polynomial fitting functions. The fitting functions are derived from spectra (in the 4000–6000 Å region) of Galactic stars and yield the line strengths as functions of stellar atmospheric parameters—metallicity, temperature, and gravity (Rose 1985; Jones 1995; Vazdekis 1999; Faber 1973; Rose 1984; Diaz et al. 1989; Worthey 1994a; Buzzoni et al. 1992, 1994; Worthey & Ottaviani 1997; Schiavon 2007; Johansson et al. 2010). The empirical polynomial fitting functions, combined with continuum levels of model SEDs, generate the absorption-line indices of SSPs.

For the standard YEPS absorption index model, we use Worthey (1994a, hereafter W94) and Worthey & Ottaviani's (1997, hereafter W97) polynomial fitting functions for 25 absorption indices of the Lick/IDS system. As a comparison model, we adopt Schiavon's (2007, hereafter S07) fitting functions in the blue wavelength based on the Jones (1999) stellar library. Figure 3 shows an example of the fitting functions (Hβ line) as given in W94 and S07. The two sets of fitting functions agree well with each other. We note that the Hβ fitting function of S07 exhibits greater metallicity sensitivity for giant stars than that of W94 by virtue of a more recent spectral library by Jones (1999).

From these fitting functions, we derive the equivalent width (EW) of a single star at a given temperature, gravity, and metallicity. The empirical fitting function provides an absorption index (I), which is transformed to the EW using the following equations:

$$\mathrm{EW}(\text{Å}) = f_C \times \left(1 - \frac{I}{\Delta\lambda}\right), \tag{5}$$

$$\mathrm{EW(mag)} = f_C \times 10^{-0.4I}, \tag{6}$$

where $\Delta\lambda$ and f_C are the index bandpass and flux continuum of an SED for each index. The continuum fluxes (f_C) of each index were taken from the definition of the Lick standard system described in W94. The unit of magnitude (mag) is used for the CN_1, CN_2, Mg_1, Mg_2, TiO_1, and TiO_2 lines.

After determining the EW and f_C of individual model stars, we finally calculate the integrated indices by summing the continua

[3] In some photometric broadband colors (e.g., $U-B$), broadband colors for an α-enhanced mixture are better reproduced by scaled-solar spectra with the same [Fe/H] of the α-enhanced mixture, not [Z/H] (Cassisi et al. 2004).

Table 2
The α-element Enhanced Patterns of Stellar Libraries

α-element	Grevesse $[\alpha/\mathrm{Fe}] = 0.0$	Y^2-Isochrones $[\alpha/\mathrm{Fe}] = 0.3$	BaSTI $[\alpha/\mathrm{Fe}] = 0.4$
C	8.55	8.55	8.55
N	7.97	7.97	7.97
O	8.87	9.17	9.37
Ne	8.08	8.38	8.37
Na	6.33	6.63	6.33
Mg	7.58	7.88	7.98
Al	6.47	6.17	6.47
Si	7.55	7.85	7.85
P	5.45	5.75	5.45
S	7.21	7.51	7.54
Cl	5.50	5.80	5.50
Ar	6.52	6.82	6.52
K	5.12	5.12	5.12
Ca	6.36	6.66	6.86
Ti	5.02	5.32	5.65
Cr	5.67	5.67	5.68
Mn	5.39	5.24	5.39
Fe	7.50	7.50	7.50
Ni	6.25	6.25	6.29

Note. The abundance of elements is listed in logarithmic scale $\log N_{\mathrm{el}}/N_{\mathrm{H}} + 12$.

and EWs of all stellar populations of SSPs using the following formulae:

$$\begin{array}{l}\text{Integrated}\\ i\text{th Index}\end{array} = \left\{ \begin{array}{l} \Delta\lambda^i \times \left(1 - \frac{\sum_j \left[f_{C,j} \times \left(1 - \frac{I_j}{\Delta\lambda^i}\right)\right]}{\sum_j f_{C,j}}\right) \\ -2.5 \log \left(\frac{\sum_j [f_{C,j} \times 10^{(-0.4 I_j)}]}{\sum_j f_{C,j}} \right) \end{array} \right\}, \qquad (7)$$

where $f_{C,j}$, I_j, and $\Delta\lambda^i$ are the jth model star's continuum, the absorption index, and the width of the ith index bandpass, respectively.

2.4. *Treatment for the Enhancement of α-elements*

The absorption indices for the case of enhanced α-elements are modeled as follows. We use Y^2 stellar evolutionary tracks with enhanced α-elements (Kim et al. 2002). For the stellar atmosphere model, we adopt the α-element mixture ratios, which are identical to those of stellar tracks for the sake of consistency. Table 2 shows the α-element mixture of the Y^2 stellar evolutionary model and BaSTI, as compared with the scaled-solar abundance ratio of metals taken from Grevesse & Noels (1993). Our YEPS models for enhanced α-elements follow the two α-element mixtures of Y^2 and BaSTI.

We then applied the response functions of α-elements by Korn et al. (2005, hereafter K05) to apply the α-element mixture to YEPS. Compared to previous work by Tripicco & Bell (1995), K05 has a more extended metallicity space ranging from [Fe/H] $= -2.25$ to $+0.67$ and provides the response functions for 25 Lick absorption indices for three evolutionary phases (dwarfs, turn-offs, and giants). The response functions that K05 provide are the first partial derivative $\partial I/\partial[X_i]$ of the Lick index I_0 when an abundance increment of two times the logarithmic ith α-element (C, N, O, Mg, Fe, Ca, Na, Si, Cr and Ti) is assumed. As described in Thomas et al. (2003, TMB03), it is appropriate to expect $I \propto \exp([X_i])$ for the optimal approximation. Hence, the Taylor expansion for $\ln I$ instead of I is an adequate approach for the variation of the Lick absorption indices due to α-element abundance changes. Neglecting the higher-order derivatives and following the notation $R_{0.3}(i)$ of Trager et al. (2000), we can express the Taylor expansion in the following forms:

$$\ln I_{\mathrm{new}} = \ln I + \sum_{i=1}^{n} \frac{\partial \ln I}{\partial [X_i]} = \ln I + \sum_{i=1}^{n} R_{0.3}(i) \frac{\Delta[X_i]}{0.3}, \qquad (8)$$

where $R_{0.3}(i) = 1/I_0 \times \partial I/\partial[X_i] \times 0.3$ is the K05 index response for increased α-element i by 0.3 dex, and I and I_0 are the absorption index before applying the K05 response function and the model absorption index of the K05 parameter space, respectively. The exponential scale of Equation (8) yields

$$I_{\mathrm{new}} = I \prod_{i=1}^{n} \exp\left(R_{0.3}(i)\right)^{\left(\frac{\Delta[X_i]}{0.3}\right)}. \qquad (9)$$

Table 3
Minimum Lick Indices Based on W94 Fitting Functions

Lick Index	Y^2 Stellar Library	BaSTI
CN_1	−0.329	−0.301
CN_2	−0.309	−0.264
Ca4227	−0.654	−0.642
G4300	−5.712	−5.712
Fe4383	−4.371	−4.377
Ca4455	−0.400	−0.404
Fe4531	−1.448	−1.417
Fe4668	−6.238	−2.156
Hβ	−1.726	−1.726
Fe5015	−0.838	−0.890
Mg_1	−0.170	−0.170
Mg_2	−0.082	−0.082
Mg b	−1.442	−1.444
Fe5270	−2.375	−2.350
Fe5335	−0.275	−0.294
Fe5406	−0.952	−0.951
Fe5709	−1.976	−1.976
Fe5782	−0.805	−0.804
NaD	0.000	0.000
TiO_1	−0.068	−0.018
TiO_2	−0.055	−0.008
Hγ_A	−12.269	−12.152
Hγ_F	−4.292	−4.278
Hδ_A	−9.384	−9.139
Hδ_F	−2.359	−2.249

Fitting functions of W94 and S07 give negative values for absorption indices when stellar populations are young and metal-poor (e.g., CN, Ca, and Fe lines) or old and metal-rich (e.g., Hβ, Hγ, and Hδ). Since our calculation of the α-element fractional change is based on the logarithmic Taylor series of $\ln I$, we must avoid negative values of the absorption indices. Table 3 lists the negative minimum values of YEPS absorption index models when we adopt W94 fitting functions together with Y^2 and BaSTI libraries. The simplest way to correct negative values in the fractional index change is to shift the negative indices into the zero or positive value and then compute the fractional change. We used the correction term δ as listed in Table 3 and applied the following equation to correct absorption

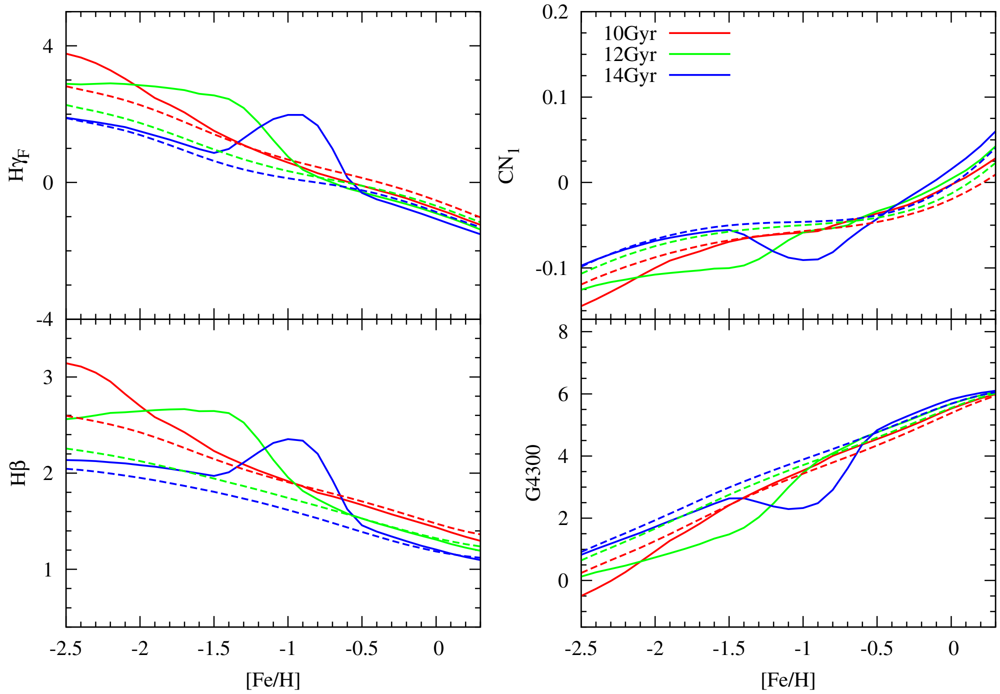

Figure 4. Effect of HB stars on the absorption indices of CN_1, G4300, $H\gamma_F$, and $H\beta$. The red, green, and blue lines indicate, respectively, SSP models with ages of 10, 12, and 14 Gyr. Solid and dashed lines are YEPS models with and without HB stars, respectively. The models are for $[\alpha/\mathrm{Fe}] = 0.3$.

indices with negative values:

$$I_{\mathrm{new}} - \delta = (I - \delta) \prod_{i=1}^{n} \exp\left(\frac{1}{I_0 - \delta} \frac{\partial I}{\partial [X_i] 0.3} \right)^{\left(\frac{\Delta [X_i]}{0.3}\right)}. \quad (10)$$

After the derivation of $I - \delta$, we scale back the index $I_{\mathrm{new}} - \delta$.

3. RESULT OF STELLAR POPULATION SIMULATIONS

3.1. The Effect of HB Stars on Simple Stellar Populations

Figure 4 shows the most temperature-sensitive indices (Balmer lines, CN_1, and G4300) as a function of [Fe/H] and highlights the effect of HB stars on the integrated absorption line strengths of SSPs. In the YEPS model without HBs, the $H\beta$ index decreases monotonically with increasing [Fe/H] at a given age. This trend is due solely to the temperature variation of the turn-off (TO) and RGB stars, which becomes cooler as the metallicity of the stellar population increases. By contrast, in the models with HB stars (solid lines), the $H\beta$ and $H\gamma_F$ strengths are significantly enhanced by the presence of blue HB stars in the metal-poor regime. CN_1 and G4300 are also sensitive to hot HB stars (W94) in the sense that these lines get weakened by the presence of hot HB stars. The models with even hotter HB stars in the most metal-poor GCs tend to approach the models without HBs, as the hotter HB stars are dim and too hot to have a significant effect on these indices.

The fact that blue HB stars can mimic young, hot TOs in the integrated fluxes of GCs has significant implication for determining ages and metallicities of stellar populations. For instance, when the $H\beta$ strength is used as an age indicator, a 7 Gyr model with no HB stars exhibits an $H\beta$ strength identical to a 12 Gyr model with HB stars at $[\mathrm{Fe/H}] \simeq -1.6$. This suggests that one could seriously underestimate the age of stellar populations for old (>10 Gyr) populations. Also, HB stars affect other absorption indices known as metallicity indicators (e.g., Mg *b*, Fe4383, and ⟨Fe⟩), although the amount of change is small compared to the Balmer indices (see Section 4 below).

Given the wide implication of the HB effect, it is highly important whether or not such an effect depends on the specific choice of stellar libraries for evolutionary tracks and the fitting functions. In this study, we employ two stellar libraries (Y^2 and BaSTI) and two empirical fitting functions (W94+W97 and S07). The four combinations of the models are presented in Figure 5. Solid and dashed lines represent the $H\beta$ strengths for the models with and without the HB prescription. A comparison shows that all models agree well with the $H\beta$ index. For instance, all the 12 Gyr models with HB stars show the same amount of $H\beta$ enhancement, about 0.6 Å at $[\mathrm{Fe/H}] \simeq -1.6$, compared to the model without HB stars. Our additional test using the high-resolution spectra of Munari et al. (2005) also confirms that, compared to the model without HBs, the model with HBs at the same condition shows enhanced $H\beta$ by about 0.6 Å. We note that the comparison between the models without HB stars (dashed lines) shows that the Y^2 stellar library produces a larger gap between iso-age lines than the BaSTI library. The reason for this is that the Y^2-isochrones have larger TO temperature gaps than the BaSTI isochrones. In addition, the fitting functions of S07 yield slightly weaker $H\beta$ indices in the metal-poor regime than W94.

3.2. The Effect of α-elements on Simple Stellar Populations

Figure 6 demonstrates the effect of α-elements on Lick indices using two indices ($H\beta$ and Mg *b*) that are sensitive to the effective temperature and α-elements, respectively. The middle column shows the effect of α-elements on $H\beta$ as functions of [Fe/H] and age. The strength of the $H\beta$ index without HB stars (dashed lines) decreases with increasing $[\alpha/\mathrm{Fe}]$. This is because the temperature of TO stars decreases with increasing $[\alpha/\mathrm{Fe}]$. Hence, the use of stellar libraries that incorporate enhanced α-elements is crucial to predict accurately the strength of $H\beta$. The total Z increment due to the α-element enhancement also

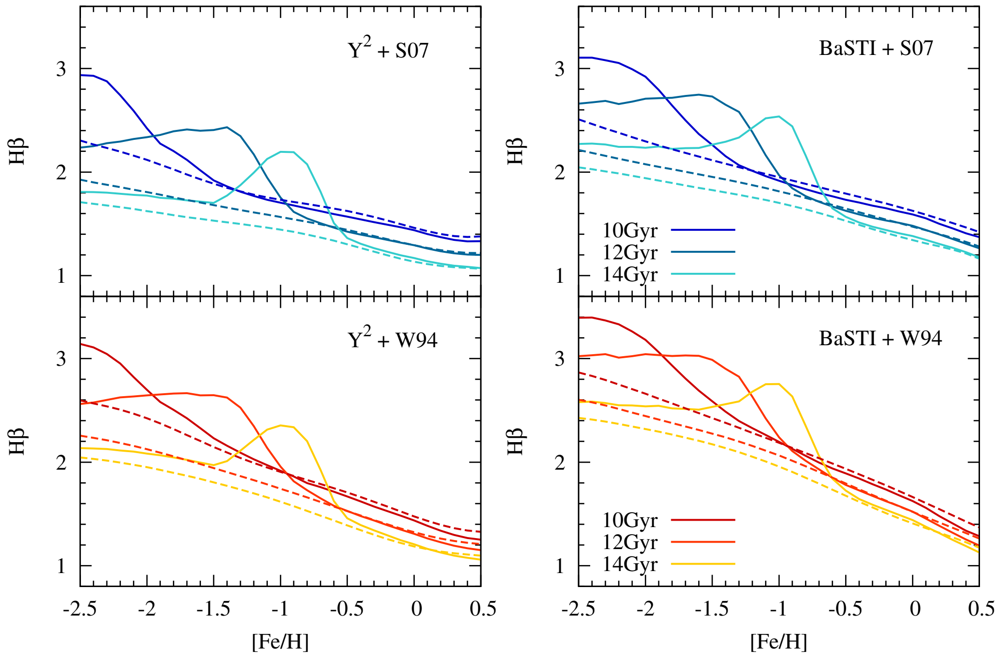

Figure 5. Effect of various input parameters (stellar libraries and fitting functions) on the strength of Hβ. The three colors indicate different ages of 10, 12, and 14 Gyr. The solid and dashed lines are YEPS models with and without HB stars. The models in the upper panels are calculated based on fitting functions of S07 and the models in the bottom panels are constructed using fitting functions of W94. Stellar evolutionary tracks used in the left and right panels are Y^2 (Kim et al. 2002) and BaSTI (Pietrinferni et al. 2004) stellar libraries, respectively.

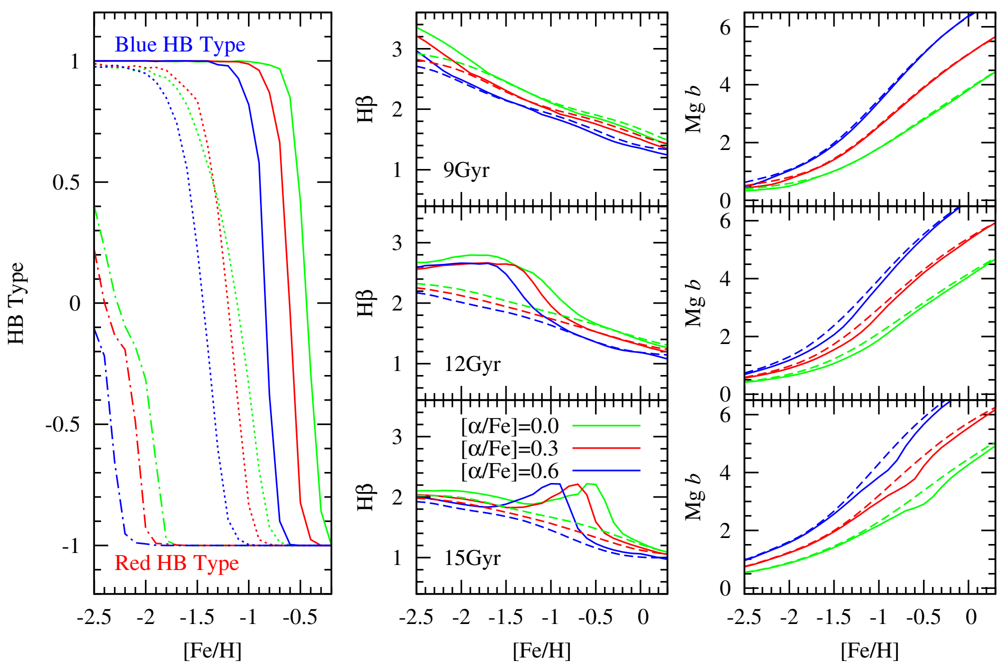

Figure 6. Effect of α-elements on the HB type, Hβ, and Mg *b* indices. The green, red, and blue colors are the YEPS models for $[\alpha/\mathrm{Fe}] = 0.0$, 0.3, and 0.6, respectively. The left panel is the same plot as Figure 1 but for various α-element enhancements. The solid, dotted, and dot-dashed lines in the left panel are HB types for three different ages of 15, 12, and 9 Gyr, respectively. The middle panels are the Hβ models with and without HB stars for different ages. The solid and dashed lines in the middle and right panels represent the YEPS models with and without HB stars. From top to bottom in the middle and right panels, the ages of the YEPS models are 9, 12, and 15 Gyr. The right panels are the YEPS models for the Mg *b* index with the same parameters as the middle panels.

affects the Hβ index with HB stars. The way the α-elements affect the HB types is shown in the left column of Figure 6. As $[\alpha/\mathrm{Fe}]$ increases, the models with enhanced $[\alpha/\mathrm{Fe}]$ (blue lines) show redder HB types compared to the scaled solar models (green lines) at a given [Fe/H]. The strengths of the Hβ index in the middle column reflect the trends on the HB types shown in the left column. Interestingly, the 15 Gyr model (solid lines in the left column) has a blue HB type at $[\mathrm{Fe/H}] = -2.5$ to -1.5, but the contribution of blue HBs to Hβ is small compared to the 12 Gyr model at the same metallicity. The first reason for this is that the strength of Hβ reaches its maximum at $T_{\mathrm{eff}} \simeq 9500$ K. So, the contribution from hotter ($T_{\mathrm{eff}} > 9500$ K) HBs in older and/or more metal-poor populations to the Hβ absorption becomes smaller. The second reason is that those HBs with a hot

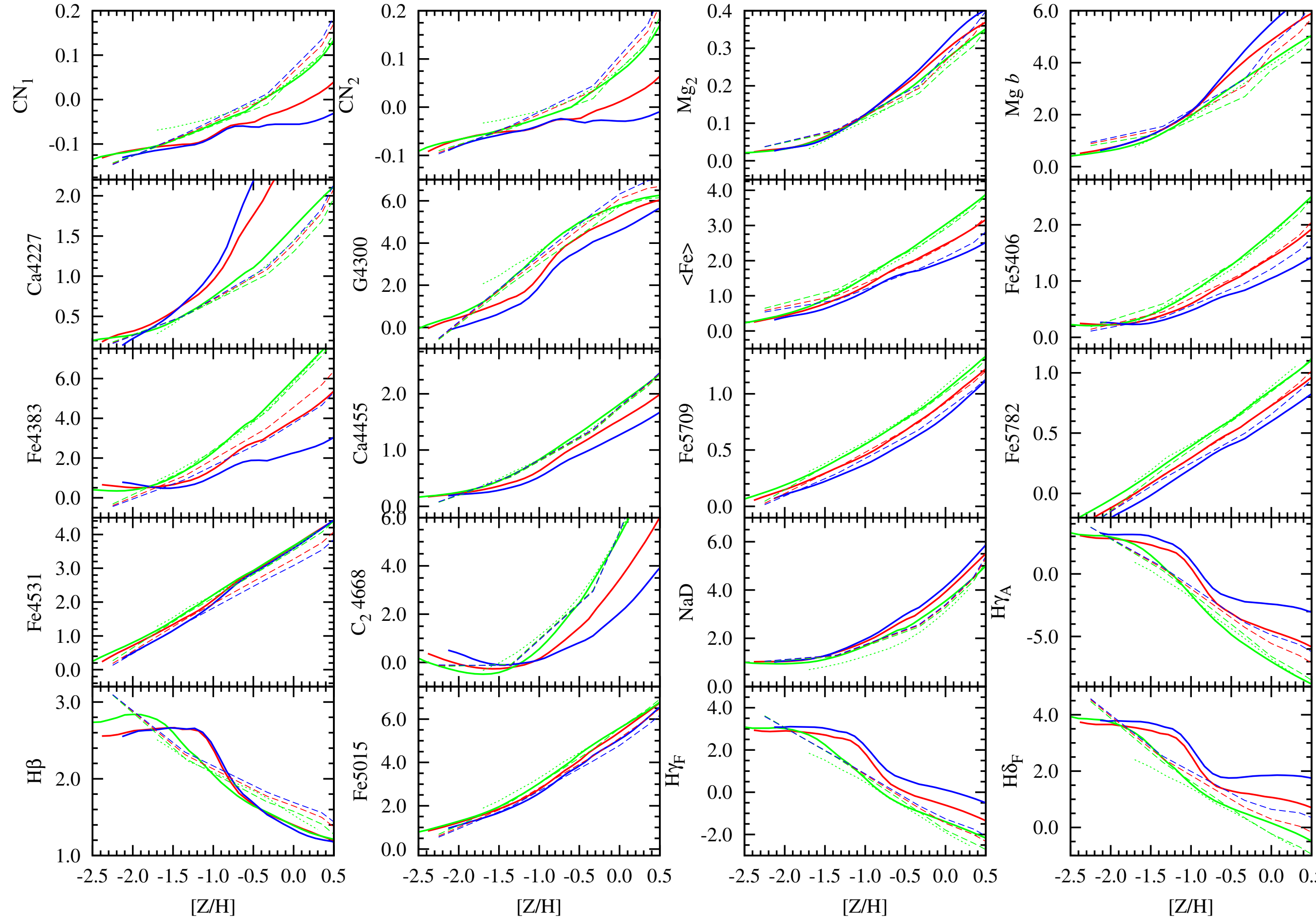

Figure 7. Comparison of the YEPS models with W94 and TMB03 models. All models are the same age of 12 Gyr. The green, red, and blue solid lines are predictions of the YEPS model for [α/Fe] = 0.0, 0.3, and 0.6, respectively. The green, red, and blue dashed lines represent TMB03 models for [α/Fe] = 0.0, 0.3, and 0.5. The dotted green lines indicate W94 models with scaled solar abundance.

temperature are fainter. Hence, their contribution to luminosity-weighted absorption indices becomes relatively small.

It is important to note that Mg *b*, the well-known tracer of [Fe/H] and [α/Fe], is also affected by the variation of HB morphologies in their absorption strengths (see 12 and 15 Gyr models). To verify the effect of HB stars on Mg *b*, we have calculated the absorption strength for the following two cases. The fitting function of S07 instead of W94 yields, for 12 Gyr SSP with [Fe/H] $\simeq -1.0$, the Mg *b* strength, which is decreased by 0.28 Å due to the effect of HB stars. The line strengths produced by high-resolution spectra of Munari et al. (2005) show that Mg *b* decreases by 0.36 Å under the same condition. The results imply that the effect of HB stars on Mg *b*, albeit relatively small compared to Hβ, is not negligible and the use of Mg *b* as a direct tracer of metallicity should be done with more caution and requires modification. It is clear that, even after the enhanced α-elements are applied to SSPs, the HB effect on the absorption indices still dominates the metal-poor regime irrespective of the [α/Fe] values.

3.3. Comparison with Other Models

In this section, we further demonstrate the characteristics of the YEPS model by comparing it with other EPS models (the W94 and TMB03 models). In order to compare the three different models simultaneously, we use the same metallicity scale [Z/H], which is defined as [Z/H] $\equiv \log(Z/Z_\odot) - \log(H/H_\odot)$, where $Z_\odot$ and $H_\odot$ are respectively the total metallicity and hydrogen content of the Sun. Figure 7 displays YEPS (solid lines), TMB03 (dashed lines), and W94 (dotted lines) models. Although the three models employ heterogeneous sets of stellar evolutionary tracks and EPS modeling schemes, they agree well with one another, except for the indices CN_1, CN_2, G4300, Hβ, Hγ, and Hδ. As discussed in previous sections, the YEPS model shows different features in these indices, because the indices are particularly sensitive to blue HB stars.

A comparison of the YEPS and TMB03 models for the α-element-enhanced cases shows that the indices insensitive to blue HBs are generally in good agreement with each other. In particular, Fe4531, Fe5015, ⟨Fe⟩, Fe5406, Fe5709, and Fe5782 agree well. However, the two models do not match for CN_1, CN_2, Ca4227, G4300, Fe4383, Ca4455, and $C_2$4668.[4] The main reasons for this difference are as follows. First, the two models use a different prescription of α-elements. The TMB03 model uses fixed C, N, and Ca with enhanced α-elements (O, Mg, Na, Ne, S, Si, and Ti) and depressed iron-peak elements (Cr, Mn, Fe, Co, Ni, Cu, and Zn). The YEPS model, on the other hand, adopts the enhanced ratios of α-elements from VandenBerg et al. (2000), i.e., fixed C and N, enhanced O, Ne, Na, Mg, Si, P, S, Cl,

[4] A comparison of the YEPS model with the most recent model of Lee et al. (2009b) shows good matches for these indices. When the age, [α/Fe], and Z of the model are assumed to be 12 Gyr, 0.3, and 0.018, respectively, compared to the scaled solar model, the index changes (ΔI) of CN_1, CN_2, Ca4227, G4300, Fe4383, Ca4455, and C_2 4668 are, respectively, −0.059, −0.061, 1.01, −0.52, −2.07, −0.28, and −1.84 for the YEPS model, and −0.054, −0.059, 0.43, −0.78, −2.37, −0.35, and −2.57 for the model of Lee et al. (2009b).

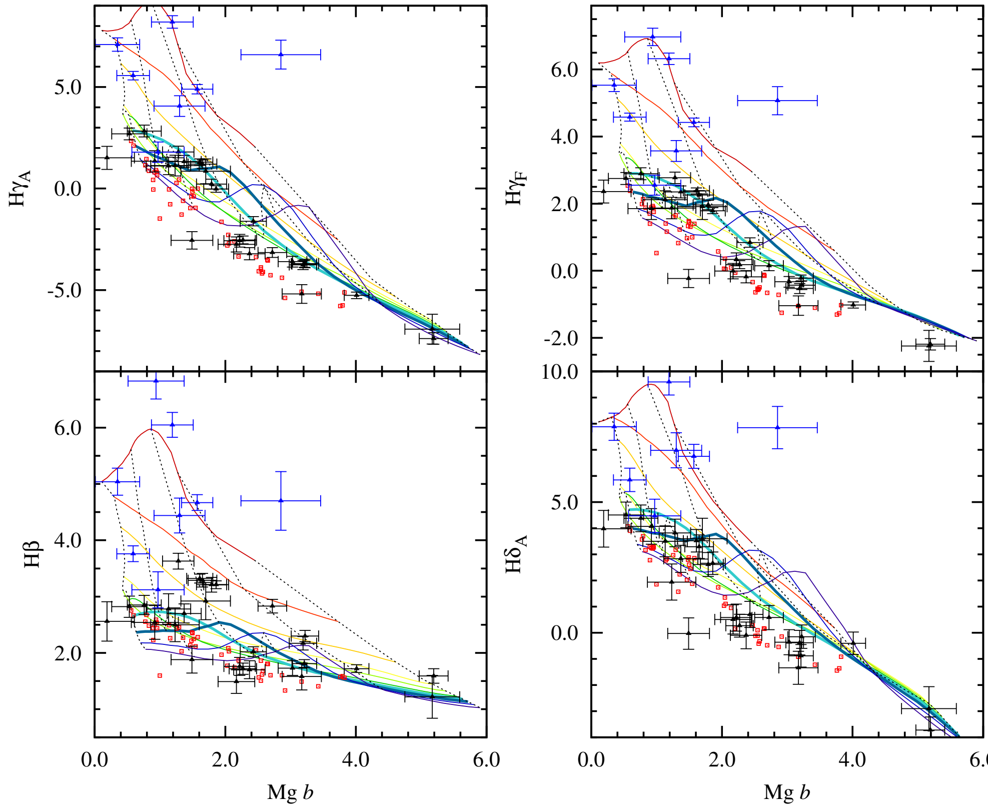

Figure 8. Comparisons of the YEPS model ([α/Fe] = 0.15) with GCs in the MW and M31. The absorption indices of Hβ, Hγ_A, Hγ_F, and Hδ_A are presented in this figure. The solid lines are the same age SSP model, and the dotted black lines indicate iso-metallicities from [Fe/H] = −2.5 to 0.5. Each solid line corresponds to an age between 1 to 15 Gyr in steps of 1 Gyr from red to blue. The thick turquoise and dark blue lines are the YEPS model for the age of 12 and 13 Gyr, respectively. The red squares are GCs in the MW observed by Schiavon et al. (2005, 2012). The black and blue triangles are GCs in M31 from Beasley et al. (2004). The blue triangles are young cluster candidates of M31 based on Beasley et al. (2004). A little offset between metal rich GCs and the model predictions for high-order Balmer indices indicates the [α/Fe] bias between metal-poor and metal-rich GCs in the MW and M31.

Ar, Ca, and Ti, and depressed Ar and Mn. The strong Ca4227 of the YEPS, for instance, can be explained by the way we treat Ca as a member of the enhanced α-element group. Second, TMB03 is based on the scaled-solar abundance isochrones (Cassisi et al. 1997; Bono et al. 1997; Salasnich et al. 2000). The model incorporates the effect of α-element enhancement by depressing iron-peak elements (e.g., Fe and Cr) in a way that satisfies the scaling relation [Z/H] = [Fe/H] + 0.94[α/Fe]. The effect of the depressed iron-peak elements is not enough to mimic the effect of stellar evolution with a depressed iron-peak elements. The YEPS model, on the other hand, uses stellar libraries with enhanced α-elements, naturally reproducing the effect of depressed iron-peak elements on iron absorption indices without adjusting the iron-peak elements in the stellar atmosphere.

3.4. Comparison with Observations: Globular Clusters in the Milky Way and M31

Figures 8–17 present the comparison of the YEPS model with the observed data on the GCs in the MW and M31. The model grids in Figures 8–12 are for various ages (solid lines) and metallicities (dotted lines). We choose [α/Fe] = 0.15[5] to consider the [α/Fe] distribution for the MWGCs (Maraston et al. 2003; Mendel et al. 2007; Woodley et al. 2010; Thomas et al. 2011) and the observed mean [α/Fe] of M31 GCs ([α/Fe] = 0.14 ± 0.04; Puzia et al. 2005). The blue triangles represent young ($\lesssim$ 1 Gyr) GC candidates in M31 (Beasley et al. 2004). Figures 13–17 exhibit the line strengths as a function of [Fe/H] for given ages but for different α-element abundance ([α/Fe] = 0.0, 0.3, and 0.6). Data for the MW and M31 GCs are obtained from Schiavon et al. (2005, 2012) and Beasley et al. (2004), respectively. For a fair comparison with old age (>12 Gyr) models, we have taken out the young M31 GC candidates (Beasley et al. 2004) in these figures. With a few exceptions, the old GCs in MW and M31 populate well along the 12 Gyr model for most indices. The theoretical predictions of the YEPS model for SSPs at 12 Gyr are given in Tables 4–6.

Notes on the individual indices shown in Figures 8–17 are as follows.

1. Hβ, Hγ_A, Hγ_F, Hδ_A, and Hδ_F. The overall shapes of model Balmer lines are in good agreement with the observation in Figures 8, 9, 13, and 14. A little offset between metal-rich GCs and the model predictions for high order Balmer indices (Figures 8 and 9) indicates the [α/Fe] bias between metal-poor and metal-rich GCs in the MW and M31 (see Figures 13 and 14). In the metal-poor regime, the 12 Gyr model GCs contain hot (>8000 K) HB stars that lead to stronger Balmer lines than the model without HB stars. The extensive study of GCs in M31 by Caldwell et al. (2011) confirms that Balmer indices of GCs with blue HBs (see their Figure 10) are on average stronger by ΔH$\beta \simeq$ 0.6 Å

[5] Recent spectroscopy of individual stars in the MWGCs confirms that the second-generation population in most clusters is depleted in oxygen (Gratton et al. 2004; Carretta et al. 2005, 2009). We can expect a similar chemical inhomogeneity in M31 GCs if the MWGCs are the local counterparts of extragalactic GCs. However, in our models for enhanced α-elements, the abundant element oxygen is included in the enhanced α-element group. This would explain why GCs in the MW show a better fit with models that have apparently lower [α/Fe] values compared to the [α/Fe] measurement based on the [Ca/Fe], [Si/Fe], and [Ti/Fe] of red giant stars in the cluster (Pritzl et al. 2005).

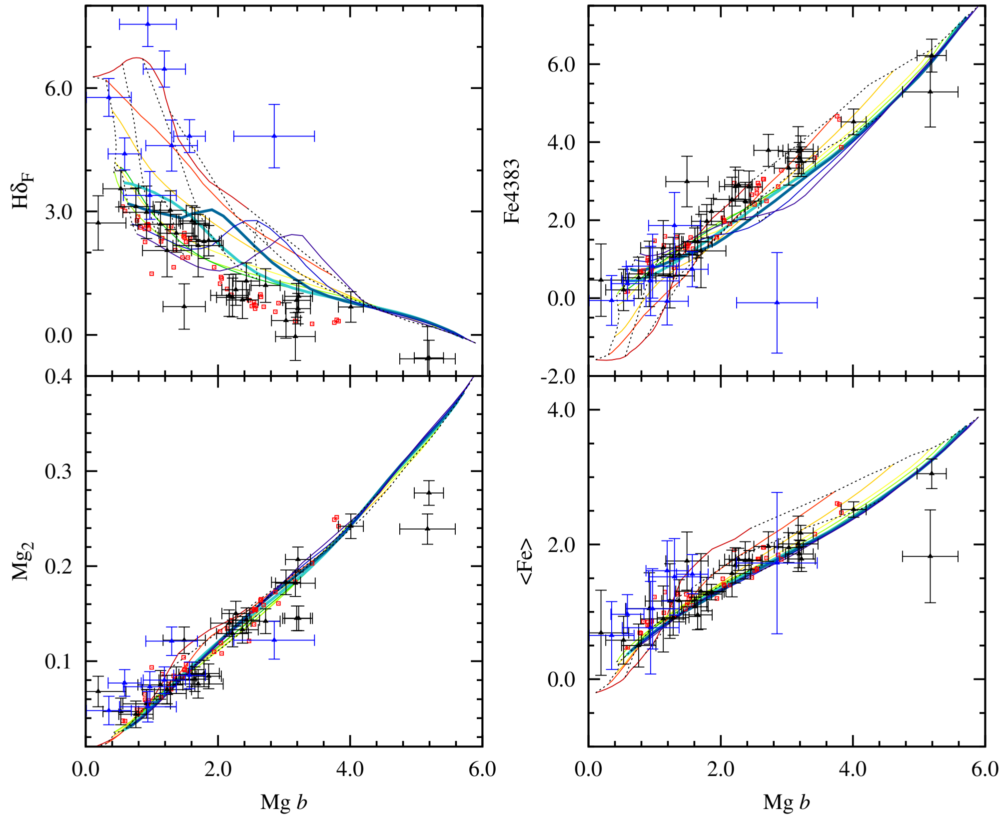

Figure 9. Same as Figure 8 but for the absorption indices of Hδ_F, Mg_2, ⟨Fe⟩, and Fe4383.

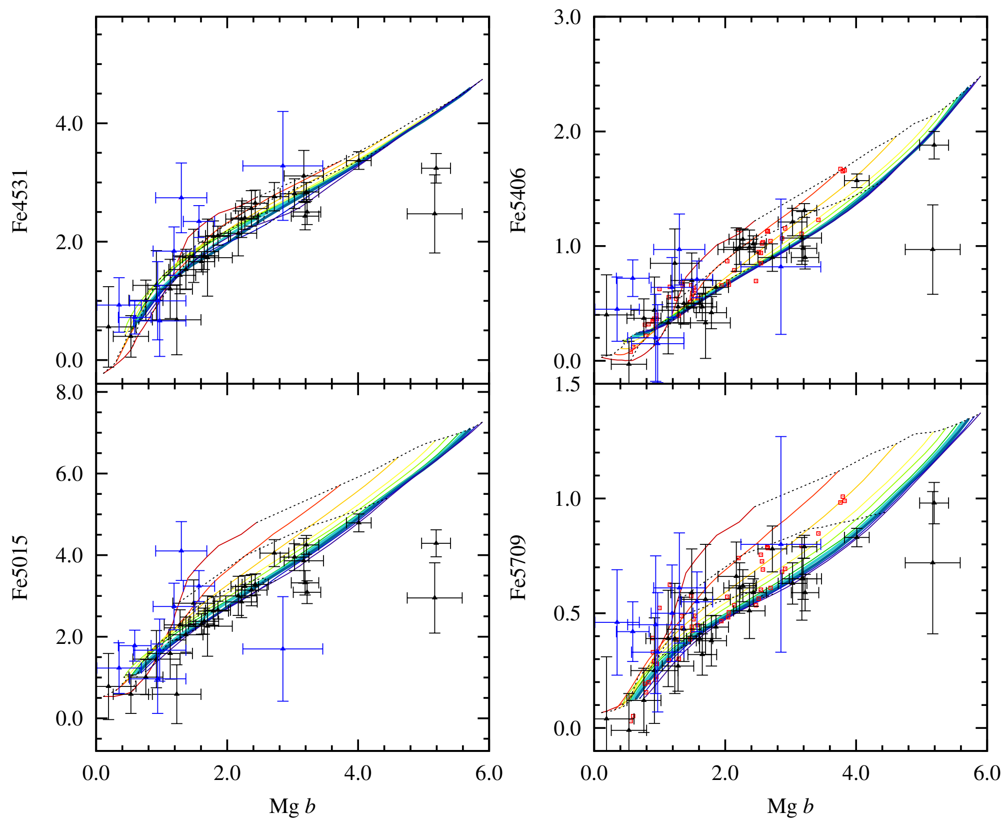

Figure 10. Same as Figure 8 but for the absorption indices of Fe4531, Fe5015, Fe5406, and Fe5709.

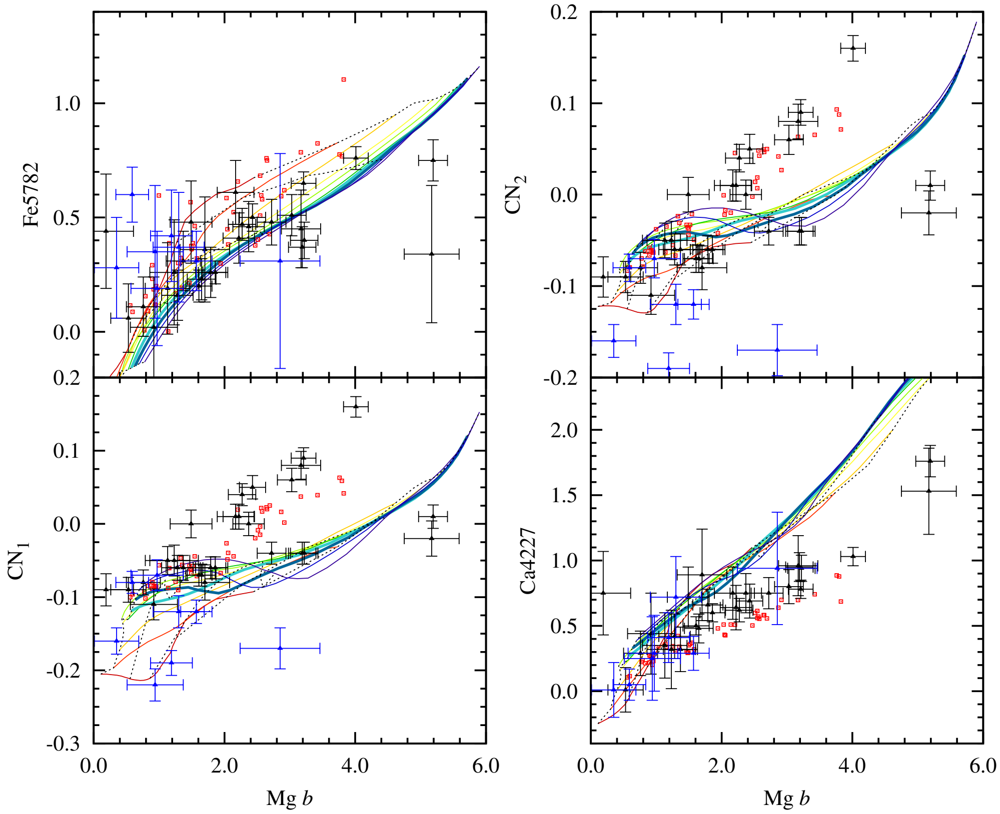

Figure 11. Same as Figure 8 but for the absorption indices of Fe5782, CN_1, CN_2, and Ca4227.

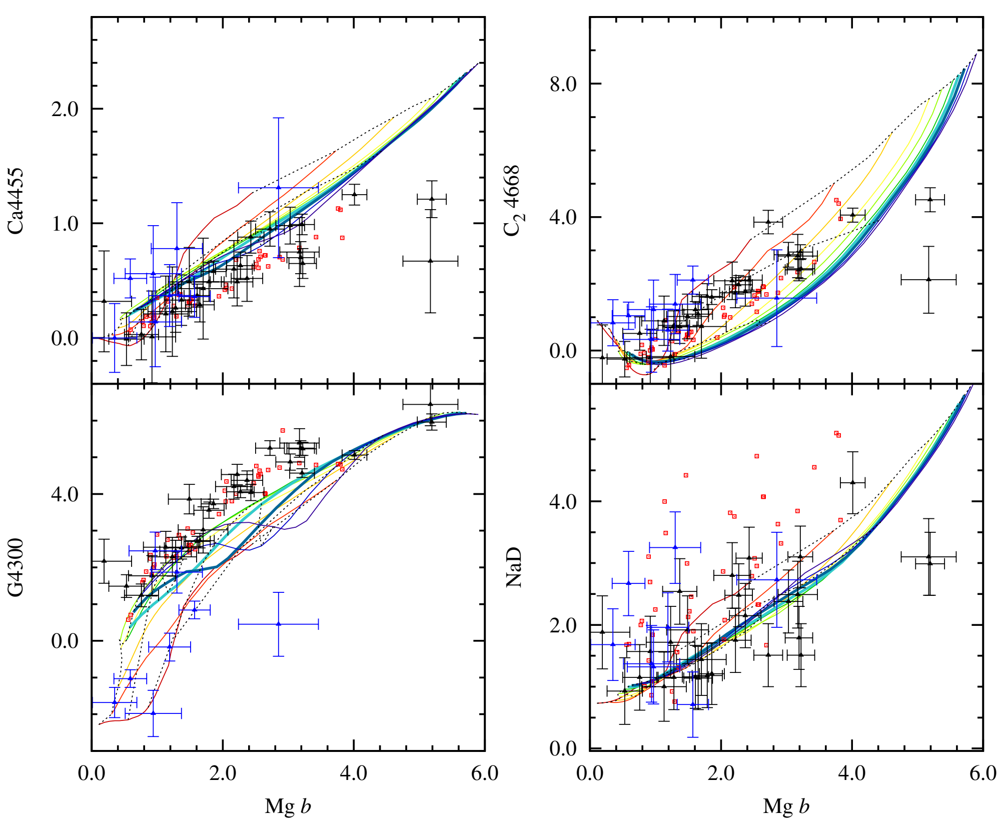

Figure 12. Same as Figure 8 but for the absorption indices of Ca4455, G4300, $C_2$4668, and NaD.

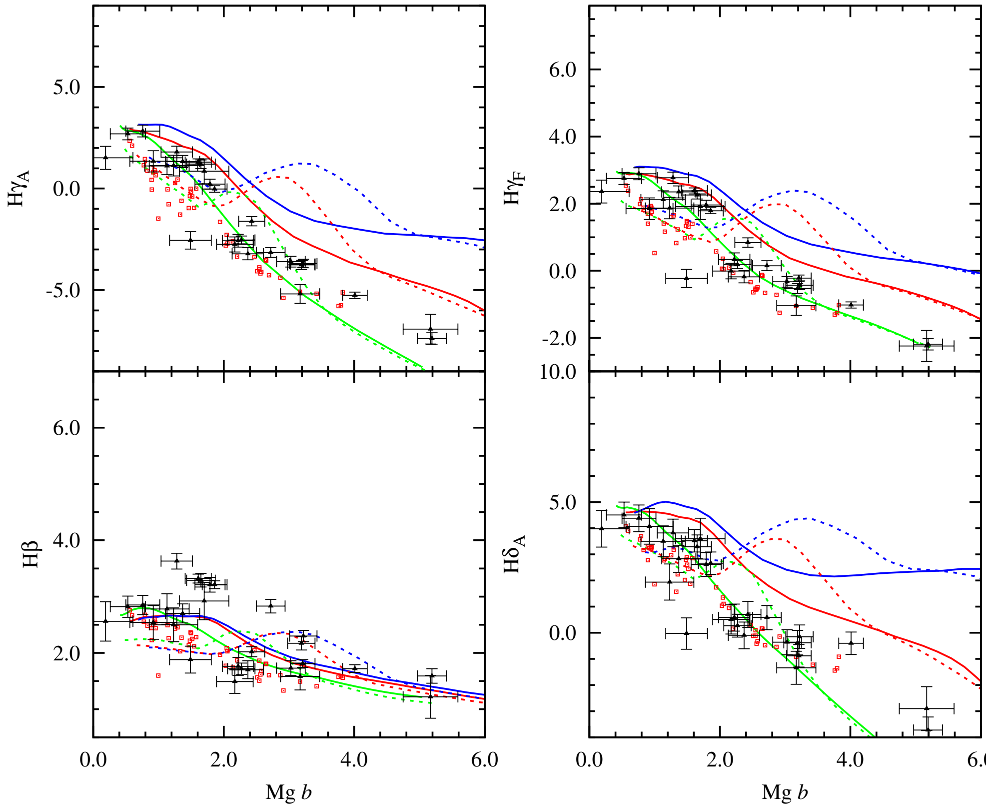

Figure 13. Comparisons between the YEPS model with enhanced α-elements and GCs in the MW and M31. The absorption indices of Hβ, Hγ_A, Hγ_F, and Hδ_A are displayed in this figure. The green, red, and blue lines represent the YEPS model for $[\alpha/\mathrm{Fe}] = 0.0$, 0.3, and 0.6, respectively. The solid and dashed lines are the YEPS models for 12 and 14 Gyr, respectively. The observed GCs are from the same data used in Figures 8–12 but we have excluded the young M31 GC candidates (blue triangles in figures 8–12) for a fair comparison with the old age (>12 Gyr) models.

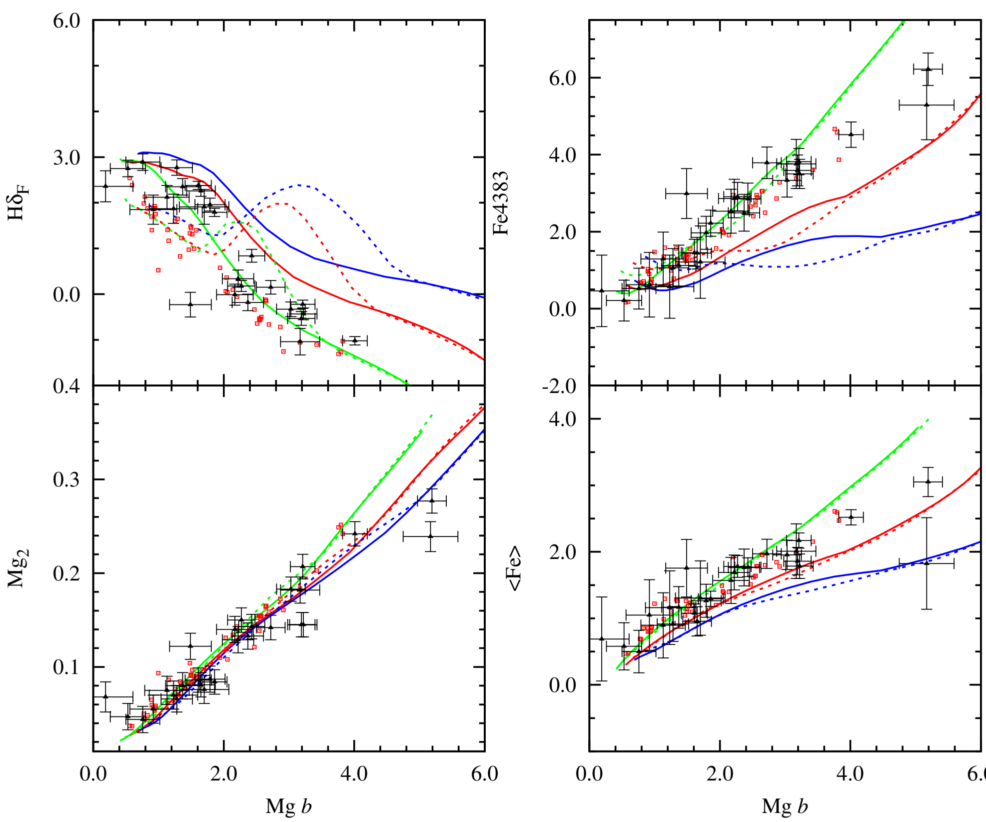

Figure 14. Same as Figure 13 but for the absorption indices of Hδ_F, Mg_2, $\langle$Fe$\rangle$, and Fe4383.

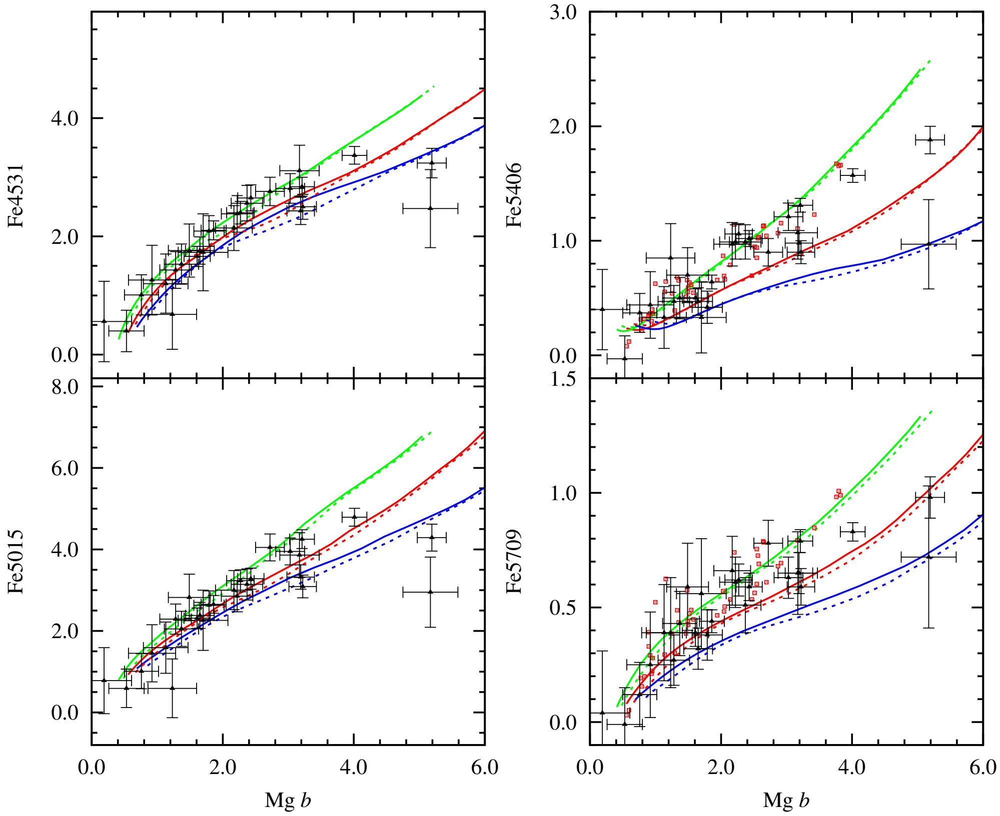

Figure 15. Same as Figure 13 but for the absorption indices of Fe4531, Fe5015, Fe5406, and Fe5709.

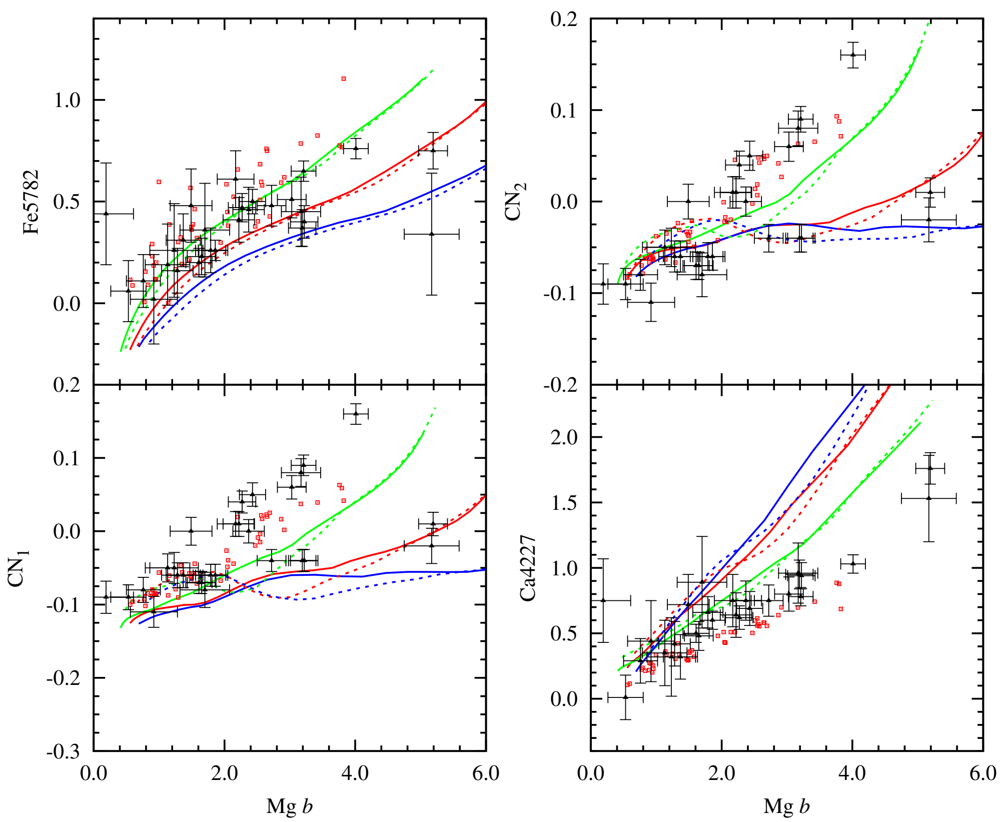

Figure 16. Same as Figure 13 but for the absorption indices of Fe5782, CN_1, CN_2, and Ca4227.

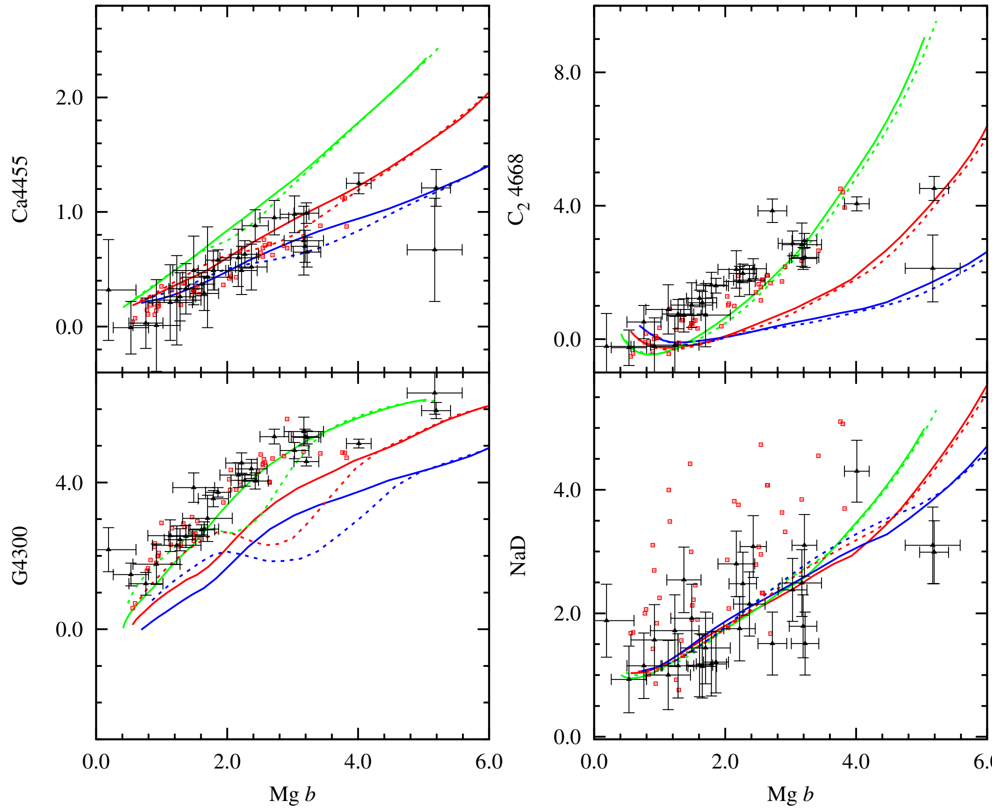

Figure 17. Same as Figure 13 but for the absorption indices of Ca4455, G4300, $C_2$4668, and NaD.

and $\Delta H\delta_F \simeq 2.0$ Å. As a consequence, the model line is highly inflected, reproducing the observed behavior of the index–index relations.

The effect of α-elements on Balmer indices differs between Hβ and higher-order Balmer indices. Figure 13 shows that Hβ is hardly affected by any α-elements. In contrast, Hδ and Hγ are sensitive to C, Mg, Fe, and total metallicity (Figures 13 and 14). The Hδ_A index is the most sensitive to α-element enhancement in the metal-rich regime because of its sensitivity to the Fe abundance in giant stars (K05). Note that the effect of HB stars on the Balmer indices is universal regardless of α-element enhancement.

2. Mg_1, Mg_2, and Mg *b*. The YEPS model well reproduces the observations of Mg_1, Mg_2, and Mg *b*. The lines are simultaneously affected by α-elements, and [α/Fe] does not change the overall shape of, for instance, the Mg *b*–Mg_2 relation (Figure 14).
3. Fe5270, Fe5335, and ⟨Fe⟩. The models and observations show remarkable agreement in Figure 9. The lines are widely used as indicators of iron abundance, yet are fairly sensitive to [α/Fe] (Figure 14).
4. Fe4383. The YEPS model well reproduces Fe4383 for GCs both in the MW and M31 (Figure 9). Since Fe4383 traces Fe and the total metallicity simultaneously, the Fe4383 model is very sensitive to variations of [α/Fe] (Figure 14).
5. Fe4531. Our model of Fe4531 agrees well with M31 GCs (Figure 10). This index is a good iron abundance indicator that is relatively less sensitive to [α/Fe] (Figure 15).
6. Fe5015. The YEPS model shows good agreement with the M31 GCs (Figure 10). The Fe5015 strength is generally involved with the Ti and Mg abundance in low MS stars and giant stars, as well as total metallicity near TOs. Yet, the effect of [α/Fe] on Fe5015 is only modest (Figure 15).
7. Fe5406, Fe5709, and Fe5782. GCs in the MW and M31 show good matches with the models. The slight offset of MWGCs in Fe5782 (Figure 11) is likely due to the well-known problem of miscalibration of fitting functions (TMB03). The α-element sensitivity of these indices is similar to those of Fe5270 and Fe5335 (Figures 15 and 16).
8. CN_1 and CN_2. The models for CN_1 and CN_2 do not show good fits to the observational data in Figure 11. Compared to observational data, our models predict on average 0.1 mag lower values in the metal-rich regime. The inferred [α/Fe] seems unreasonably high and likely due to the poor calibration of fitting functions (TMB03; Lee & Worthey 2005). The poor calibration of fitting functions can be explained by the effect of the CNONa anticorrelation found in the MWGCs with the second-generation stellar population (Coelho et al. 2011). CN_1 and CN_2 indices, even for the α-element-enhanced models, are fairly affected by blue HB stars (see solid and dashed lines in Figure 16).
9. Ca4227. Our models for Ca4227 show a small offset from the observations. The observations occupy slightly lower EWs compared to the model in Figures 11 and 16. As suggested by TMB03 and Lee et al. (2009a), the enhanced C and N model can depress EW of Ca4227, but we do not consider the case of the enhanced C and N model in this study. Note that a more realistic model with the effect of the CNONa anticorrelation would have decreased the strength of Ca4227 (Coelho et al. 2011), and this may explain the offset between the YEPS model and the observations. Since Ca4227 is very sensitive to Ca and C but not to Mg, the Ca4227 line deepens with increasing [α/Fe] (Figure 16).
10. Ca4455. The Ca4455 model for [α/Fe] = 0.15 predicts on average 0.3 Å higher EWs compared to the observations (Figure 12), and the observations are better reproduced by

Table 4
LICK Absorption Indices of YEPS Simple Stellar Population Model for [α/Fe] = 0.0 (Fitting Functions of W94 and W97)

Age = 12.0

[Fe/H]	CN_1	CN_2	Ca4227	G4300	Fe4383	Ca4455	Fe4531	$C_2$4668	Hβ	Fe5015	Mg_1	Mg_2
−2.50	−0.132	−0.089	0.213	0.033	0.451	0.166	0.258	0.156	2.672	0.798	0.007	0.021
−2.40	−0.126	−0.082	0.230	0.207	0.426	0.181	0.378	0.010	2.673	0.885	0.007	0.023
−2.30	−0.121	−0.076	0.242	0.342	0.401	0.196	0.490	−0.100	2.693	0.982	0.006	0.024
−2.20	−0.118	−0.072	0.256	0.465	0.393	0.214	0.600	−0.202	2.719	1.086	0.006	0.026
−2.10	−0.116	−0.069	0.265	0.563	0.390	0.232	0.703	−0.285	2.758	1.188	0.006	0.028
−2.00	−0.114	−0.065	0.281	0.688	0.421	0.254	0.813	−0.359	2.775	1.292	0.007	0.032
−1.90	−0.112	−0.063	0.298	0.810	0.468	0.278	0.922	−0.417	2.794	1.399	0.008	0.035
−1.80	−0.110	−0.060	0.320	0.958	0.543	0.308	1.035	−0.454	2.792	1.514	0.010	0.040
−1.70	−0.107	−0.058	0.344	1.104	0.637	0.341	1.149	−0.465	2.793	1.633	0.012	0.046
−1.60	−0.104	−0.055	0.378	1.301	0.768	0.382	1.273	−0.453	2.765	1.771	0.015	0.053
−1.50	−0.099	−0.052	0.418	1.538	0.931	0.431	1.405	−0.406	2.712	1.926	0.018	0.061
−1.40	−0.094	−0.049	0.467	1.813	1.119	0.489	1.545	−0.312	2.630	2.103	0.021	0.070
−1.30	−0.089	−0.045	0.517	2.080	1.320	0.550	1.683	−0.179	2.556	2.292	0.026	0.081
−1.20	−0.084	−0.042	0.566	2.339	1.527	0.613	1.816	−0.018	2.499	2.487	0.030	0.092
−1.10	−0.076	−0.037	0.634	2.718	1.799	0.695	1.976	0.202	2.376	2.719	0.035	0.104
−1.00	−0.066	−0.030	0.705	3.147	2.094	0.785	2.140	0.468	2.226	2.962	0.040	0.117
−0.90	−0.055	−0.022	0.787	3.606	2.448	0.886	2.313	0.799	2.068	3.227	0.046	0.131
−0.80	−0.045	−0.015	0.868	4.028	2.844	0.989	2.479	1.176	1.939	3.492	0.053	0.145
−0.70	−0.035	−0.007	0.959	4.417	3.277	1.099	2.648	1.613	1.815	3.773	0.060	0.158
−0.60	−0.028	−0.001	1.040	4.695	3.658	1.200	2.799	2.054	1.730	4.038	0.068	0.172
−0.50	−0.018	0.008	1.108	4.946	3.952	1.295	2.932	2.463	1.660	4.332	0.074	0.185
−0.40	−0.003	0.023	1.182	5.171	4.269	1.394	3.069	2.940	1.604	4.634	0.079	0.199
−0.30	0.009	0.036	1.286	5.346	4.696	1.499	3.223	3.516	1.556	4.886	0.086	0.217
−0.20	0.020	0.048	1.392	5.509	5.117	1.604	3.374	4.078	1.501	5.125	0.096	0.234
−0.10	0.031	0.060	1.500	5.659	5.530	1.708	3.521	4.646	1.446	5.355	0.105	0.252
0.00	0.043	0.072	1.607	5.798	5.943	1.813	3.666	5.243	1.392	5.581	0.116	0.269
0.10	0.056	0.086	1.712	5.924	6.353	1.917	3.809	5.875	1.344	5.805	0.126	0.287
0.20	0.071	0.102	1.816	6.037	6.767	2.023	3.953	6.565	1.302	6.034	0.136	0.303
0.30	0.087	0.119	1.918	6.132	7.177	2.128	4.095	7.308	1.267	6.266	0.146	0.320
0.40	0.108	0.141	2.018	6.209	7.590	2.236	4.241	8.136	1.238	6.516	0.155	0.336
0.50	0.134	0.169	2.113	6.260	8.007	2.344	4.389	9.057	1.213	6.779	0.164	0.352

[Fe/H]	Mg *b*	Fe5270	Fe5335	Fe5406	Fe5709	Fe5782	NaD	$H\gamma_A$	$H\gamma_F$	$H\delta_A$	$H\delta_F$
−2.50	0.411	−0.137	0.606	0.227	0.066	−0.238	1.001	3.106	2.968	4.869	3.830
−2.40	0.446	−0.031	0.592	0.216	0.089	−0.201	0.976	2.966	2.911	4.807	3.764
−2.30	0.487	0.070	0.584	0.211	0.113	−0.163	0.961	2.881	2.896	4.782	3.739
−2.20	0.531	0.172	0.582	0.211	0.137	−0.126	0.952	2.837	2.898	4.779	3.721
−2.10	0.578	0.271	0.585	0.216	0.163	−0.088	0.949	2.838	2.927	4.801	3.721
−2.00	0.634	0.374	0.597	0.227	0.191	−0.050	0.952	2.784	2.915	4.771	3.681
−1.90	0.696	0.478	0.617	0.245	0.220	−0.010	0.963	2.729	2.901	4.738	3.638
−1.80	0.771	0.586	0.648	0.271	0.252	0.031	0.984	2.610	2.847	4.657	3.565
−1.70	0.855	0.696	0.689	0.305	0.284	0.073	1.017	2.481	2.789	4.564	3.488
−1.60	0.951	0.814	0.742	0.348	0.317	0.115	1.065	2.247	2.670	4.383	3.356
−1.50	1.062	0.938	0.808	0.399	0.351	0.159	1.127	1.909	2.495	4.119	3.178
−1.40	1.196	1.073	0.890	0.461	0.388	0.205	1.208	1.484	2.271	3.795	2.969
−1.30	1.348	1.208	0.980	0.528	0.425	0.250	1.303	1.046	2.052	3.479	2.779
−1.20	1.498	1.338	1.075	0.597	0.460	0.293	1.410	0.637	1.861	3.160	2.591
−1.10	1.678	1.487	1.189	0.679	0.498	0.338	1.533	−0.051	1.521	2.619	2.280
−1.00	1.878	1.640	1.314	0.765	0.538	0.382	1.665	−0.868	1.108	1.979	1.911
−0.90	2.113	1.804	1.456	0.863	0.581	0.428	1.815	−1.796	0.650	1.296	1.546
−0.80	2.352	1.968	1.603	0.964	0.625	0.474	1.976	−2.687	0.225	0.650	1.248
−0.70	2.597	2.138	1.764	1.075	0.675	0.521	2.153	−3.548	−0.167	−0.022	0.996
−0.60	2.825	2.294	1.918	1.182	0.722	0.565	2.332	−4.178	−0.423	−0.563	0.834
−0.50	3.042	2.429	2.047	1.279	0.772	0.605	2.465	−4.757	−0.631	−1.035	0.701
−0.40	3.251	2.568	2.183	1.383	0.821	0.652	2.607	−5.301	−0.815	−1.513	0.573
−0.30	3.458	2.723	2.358	1.501	0.867	0.705	2.828	−5.747	−0.965	−1.984	0.468
−0.20	3.658	2.871	2.534	1.619	0.919	0.756	3.057	−6.181	−1.109	−2.441	0.364
−0.10	3.857	3.016	2.712	1.737	0.974	0.806	3.296	−6.598	−1.251	−2.886	0.259
0.00	4.064	3.158	2.893	1.857	1.032	0.855	3.542	−7.004	−1.392	−3.331	0.152
0.10	4.272	3.297	3.078	1.979	1.089	0.903	3.804	−7.392	−1.536	−3.771	0.041
0.20	4.473	3.437	3.270	2.105	1.150	0.952	4.078	−7.769	−1.688	−4.212	−0.077
0.30	4.672	3.575	3.468	2.234	1.210	0.999	4.368	−8.122	−1.841	−4.635	−0.197
0.40	4.864	3.716	3.675	2.367	1.271	1.051	4.672	−8.468	−2.004	−5.057	−0.331
0.50	5.044	3.864	3.890	2.500	1.334	1.105	4.996	−8.791	−2.165	−5.469	−0.481

Note. The entire data of Table 4 are available at http://web.yonsei.ac.kr/cosmic/data/YEPS.htm.

Table 5
LICK Absorption Indices of YEPS Simple Stellar Population Model for [α/Fe] = 0.3 (Fitting Functions of W94 and W97)

Age = 12.0

[Fe/H]	CN_1	CN_2	Ca4227	G4300	Fe4383	Ca4455	Fe4531	$C_2$4668	Hβ	Fe5015	Mg_1	Mg_2
−2.50	−0.125	−0.084	0.235	0.122	0.611	0.184	0.371	0.242	2.561	0.930	0.008	0.027
−2.40	−0.120	−0.077	0.274	0.264	0.570	0.199	0.500	0.116	2.576	1.033	0.008	0.029
−2.30	−0.117	−0.071	0.298	0.372	0.529	0.215	0.618	0.010	2.601	1.140	0.008	0.031
−2.20	−0.114	−0.067	0.322	0.475	0.502	0.231	0.733	−0.080	2.626	1.251	0.008	0.033
−2.10	−0.110	−0.062	0.356	0.606	0.505	0.252	0.855	−0.157	2.634	1.367	0.009	0.037
−2.00	−0.108	−0.059	0.399	0.738	0.517	0.275	0.977	−0.214	2.644	1.484	0.011	0.042
−1.90	−0.106	−0.056	0.450	0.872	0.549	0.301	1.101	−0.248	2.654	1.607	0.014	0.049
−1.80	−0.104	−0.054	0.507	1.016	0.602	0.332	1.230	−0.265	2.662	1.738	0.017	0.057
−1.70	−0.103	−0.052	0.568	1.164	0.674	0.366	1.358	−0.257	2.666	1.875	0.021	0.066
−1.60	−0.101	−0.050	0.640	1.345	0.777	0.407	1.493	−0.222	2.644	2.030	0.025	0.076
−1.50	−0.100	−0.049	0.704	1.482	0.874	0.447	1.616	−0.163	2.646	2.185	0.029	0.087
−1.40	−0.097	−0.048	0.775	1.696	1.023	0.498	1.754	−0.095	2.624	2.362	0.033	0.099
−1.30	−0.090	−0.044	0.863	2.032	1.230	0.564	1.911	0.019	2.526	2.569	0.037	0.112
−1.20	−0.079	−0.038	0.972	2.481	1.474	0.647	2.089	0.179	2.348	2.805	0.041	0.126
−1.10	−0.067	−0.031	1.104	2.994	1.752	0.744	2.279	0.400	2.137	3.068	0.046	0.142
−1.00	−0.059	−0.026	1.275	3.464	2.074	0.847	2.470	0.659	1.956	3.348	0.053	0.158
−0.90	−0.055	−0.025	1.480	3.836	2.386	0.950	2.648	0.922	1.815	3.622	0.060	0.174
−0.80	−0.053	−0.025	1.638	4.089	2.626	1.036	2.796	1.209	1.728	3.864	0.067	0.190
−0.70	−0.050	−0.023	1.786	4.327	2.793	1.117	2.932	1.489	1.650	4.129	0.074	0.206
−0.60	−0.041	−0.014	1.937	4.583	2.916	1.200	3.070	1.796	1.579	4.448	0.079	0.222
−0.50	−0.034	−0.006	2.124	4.766	3.183	1.291	3.229	2.240	1.529	4.705	0.087	0.242
−0.40	−0.028	−0.001	2.299	4.942	3.432	1.375	3.377	2.642	1.480	4.940	0.095	0.262
−0.30	−0.022	0.005	2.466	5.121	3.687	1.461	3.526	3.066	1.436	5.182	0.104	0.280
−0.20	−0.014	0.012	2.647	5.315	3.918	1.544	3.682	3.513	1.391	5.443	0.113	0.298
−0.10	−0.006	0.020	2.815	5.503	4.157	1.628	3.838	3.984	1.348	5.709	0.121	0.315
0.00	0.004	0.030	2.966	5.684	4.423	1.717	3.996	4.488	1.308	5.986	0.129	0.331
0.10	0.014	0.039	3.079	5.824	4.721	1.806	4.144	4.988	1.264	6.246	0.136	0.346
0.20	0.027	0.051	3.169	5.951	5.055	1.902	4.290	5.529	1.226	6.519	0.142	0.359
0.30	0.042	0.067	3.241	6.056	5.425	2.004	4.434	6.111	1.192	6.797	0.147	0.372
0.40	0.059	0.084	3.294	6.131	5.785	2.102	4.558	6.760	1.168	7.062	0.152	0.383
0.50	0.079	0.105	3.349	6.172	6.135	2.199	4.667	7.486	1.150	7.301	0.159	0.396

[Fe/H]	Mg *b*	Fe5270	Fe5335	Fe5406	Fe5709	Fe5782	NaD	Hγ_A	Hγ_F	Hδ_A	Hδ_F
−2.50	0.556	−0.050	0.649	0.237	0.080	−0.229	1.032	2.945	2.886	4.603	3.685
−2.40	0.611	0.060	0.636	0.228	0.104	−0.189	1.033	2.870	2.870	4.604	3.656
−2.30	0.672	0.165	0.627	0.222	0.127	−0.151	1.034	2.843	2.887	4.631	3.655
−2.20	0.737	0.269	0.622	0.221	0.152	−0.113	1.042	2.821	2.903	4.657	3.652
−2.10	0.812	0.379	0.628	0.228	0.178	−0.074	1.060	2.743	2.879	4.642	3.614
−2.00	0.895	0.489	0.641	0.242	0.207	−0.035	1.093	2.656	2.848	4.632	3.576
−1.90	0.992	0.602	0.665	0.265	0.237	0.006	1.142	2.553	2.808	4.616	3.536
−1.80	1.101	0.718	0.699	0.295	0.268	0.049	1.207	2.441	2.760	4.592	3.482
−1.70	1.226	0.834	0.741	0.333	0.299	0.091	1.288	2.296	2.702	4.543	3.426
−1.60	1.376	0.959	0.797	0.379	0.332	0.134	1.386	2.070	2.598	4.431	3.337
−1.50	1.539	1.075	0.856	0.428	0.363	0.176	1.496	1.921	2.549	4.371	3.297
−1.40	1.709	1.197	0.924	0.480	0.394	0.218	1.612	1.671	2.442	4.205	3.172
−1.30	1.903	1.331	1.004	0.540	0.425	0.259	1.739	1.134	2.182	3.777	2.898
−1.20	2.133	1.479	1.100	0.608	0.460	0.302	1.879	0.326	1.751	3.130	2.479
−1.10	2.419	1.639	1.210	0.687	0.499	0.347	2.036	−0.636	1.239	2.418	2.024
−1.00	2.744	1.804	1.330	0.774	0.544	0.392	2.219	−1.593	0.756	1.797	1.680
−0.90	3.069	1.960	1.449	0.862	0.592	0.437	2.416	−2.361	0.377	1.302	1.459
−0.80	3.364	2.088	1.554	0.941	0.636	0.477	2.618	−2.823	0.168	0.980	1.355
−0.70	3.650	2.199	1.639	1.013	0.682	0.511	2.793	−3.220	−0.005	0.733	1.287
−0.60	3.929	2.301	1.711	1.084	0.733	0.550	2.929	−3.628	−0.172	0.510	1.229
−0.50	4.200	2.428	1.832	1.176	0.778	0.600	3.175	−3.889	−0.284	0.287	1.194
−0.40	4.446	2.546	1.950	1.261	0.828	0.646	3.422	−4.131	−0.399	0.085	1.147
−0.30	4.676	2.666	2.074	1.349	0.882	0.691	3.683	−4.381	−0.513	−0.138	1.098
−0.20	4.893	2.782	2.191	1.433	0.939	0.736	3.970	−4.593	−0.633	−0.312	1.057
−0.10	5.114	2.899	2.318	1.519	0.997	0.780	4.276	−4.804	−0.759	−0.498	1.012
0.00	5.333	3.024	2.457	1.614	1.057	0.825	4.593	−5.038	−0.899	−0.722	0.954
0.10	5.547	3.150	2.612	1.716	1.113	0.871	4.915	−5.280	−1.045	−0.981	0.882
0.20	5.747	3.284	2.781	1.826	1.171	0.919	5.239	−5.561	−1.203	−1.304	0.794
0.30	5.929	3.426	2.965	1.946	1.231	0.971	5.566	−5.881	−1.376	−1.691	0.685
0.40	6.089	3.563	3.147	2.064	1.285	1.019	5.876	−6.171	−1.536	−2.071	0.571
0.50	6.214	3.698	3.326	2.179	1.336	1.067	6.168	−6.443	−1.694	−2.448	0.439

Note. The entire data of Table 5 are available at http://web.yonsei.ac.kr/cosmic/data/YEPS.htm.

Table 6
LICK Absorption Indices of YEPS Simple Stellar Population Model for [α/Fe] = 0.6 (Fitting Functions of W94 and W97)

Age = 12.0

[Fe/H]	CN_1	CN_2	Ca4227	G4300	Fe4383	Ca4455	Fe4531	$C_2$4668	Hβ	Fe5015	Mg_1	Mg_2
−2.50	−0.126	−0.082	0.207	−0.015	0.733	0.206	0.464	0.409	2.587	1.073	0.010	0.031
−2.40	−0.123	−0.076	0.264	0.092	0.656	0.218	0.593	0.288	2.622	1.179	0.011	0.035
−2.30	−0.119	−0.071	0.319	0.216	0.583	0.227	0.721	0.156	2.630	1.284	0.010	0.037
−2.20	−0.115	−0.066	0.378	0.340	0.519	0.239	0.848	0.043	2.635	1.393	0.011	0.041
−2.10	−0.113	−0.062	0.443	0.460	0.477	0.254	0.978	−0.040	2.651	1.507	0.013	0.047
−2.00	−0.110	−0.059	0.518	0.600	0.473	0.275	1.114	−0.092	2.663	1.635	0.016	0.055
−1.90	−0.107	−0.055	0.603	0.769	0.516	0.306	1.259	−0.102	2.657	1.780	0.020	0.065
−1.80	−0.104	−0.052	0.696	0.951	0.589	0.342	1.408	−0.083	2.648	1.938	0.025	0.077
−1.70	−0.102	−0.049	0.787	1.119	0.678	0.381	1.553	−0.045	2.657	2.103	0.030	0.090
−1.60	−0.096	−0.045	0.896	1.396	0.827	0.433	1.716	0.009	2.605	2.294	0.035	0.104
−1.50	−0.087	−0.040	1.025	1.782	1.015	0.497	1.896	0.077	2.481	2.504	0.040	0.119
−1.40	−0.077	−0.034	1.175	2.247	1.215	0.574	2.089	0.182	2.295	2.740	0.045	0.134
−1.30	−0.066	−0.027	1.363	2.730	1.433	0.661	2.293	0.334	2.094	3.004	0.051	0.152
−1.20	−0.060	−0.024	1.631	3.099	1.637	0.750	2.501	0.484	1.926	3.297	0.057	0.169
−1.10	−0.060	−0.026	1.892	3.378	1.791	0.831	2.677	0.629	1.802	3.551	0.064	0.187
−1.00	−0.061	−0.030	2.120	3.587	1.880	0.898	2.821	0.779	1.714	3.773	0.071	0.205
−0.90	−0.062	−0.032	2.347	3.814	1.887	0.961	2.956	0.913	1.621	4.019	0.077	0.223
−0.80	−0.057	−0.028	2.585	4.059	1.863	1.029	3.099	1.106	1.533	4.316	0.082	0.243
−0.70	−0.056	−0.027	2.838	4.223	1.981	1.102	3.251	1.397	1.473	4.548	0.089	0.264
−0.60	−0.056	−0.028	3.088	4.383	2.098	1.175	3.400	1.672	1.413	4.770	0.099	0.287
−0.50	−0.056	−0.029	3.334	4.545	2.225	1.249	3.548	1.960	1.357	4.992	0.108	0.309
−0.40	−0.056	−0.029	3.602	4.717	2.329	1.321	3.702	2.256	1.301	5.226	0.119	0.331
−0.30	−0.053	−0.027	3.857	4.923	2.452	1.398	3.866	2.594	1.257	5.497	0.128	0.352
−0.20	−0.048	−0.023	4.093	5.150	2.583	1.475	4.037	2.977	1.225	5.803	0.137	0.370
−0.10	−0.042	−0.018	4.295	5.374	2.748	1.557	4.209	3.386	1.202	6.124	0.144	0.386
0.00	−0.033	−0.011	4.463	5.599	2.964	1.644	4.380	3.808	1.186	6.458	0.148	0.399
0.10	−0.026	−0.005	4.561	5.749	3.237	1.732	4.534	4.167	1.155	6.751	0.151	0.411
0.20	−0.016	0.003	4.645	5.880	3.567	1.835	4.696	4.536	1.121	7.067	0.152	0.421
0.30	−0.003	0.015	4.746	5.974	3.971	1.961	4.874	4.888	1.079	7.392	0.156	0.434

[Fe/H]	Mg *b*	Fe5270	Fe5335	Fe5406	Fe5709	Fe5782	NaD	Hγ_A	Hγ_F	Hδ_A	Hδ_F
−2.50	0.689	0.031	0.715	0.261	0.097	−0.214	1.054	3.152	3.079	4.586	3.776
−2.40	0.767	0.139	0.697	0.250	0.120	−0.175	1.078	3.138	3.103	4.658	3.783
−2.30	0.855	0.239	0.673	0.236	0.142	−0.140	1.097	3.142	3.098	4.759	3.772
−2.20	0.952	0.339	0.655	0.228	0.164	−0.104	1.127	3.146	3.086	4.872	3.764
−2.10	1.057	0.444	0.650	0.231	0.187	−0.067	1.176	3.139	3.081	4.974	3.756
−2.00	1.174	0.559	0.663	0.246	0.213	−0.027	1.250	3.050	3.048	5.011	3.722
−1.90	1.313	0.687	0.694	0.275	0.241	0.016	1.350	2.853	2.973	4.950	3.652
−1.80	1.471	0.821	0.739	0.314	0.271	0.060	1.471	2.600	2.883	4.834	3.567
−1.70	1.643	0.952	0.792	0.357	0.300	0.104	1.607	2.381	2.827	4.732	3.498
−1.60	1.838	1.095	0.855	0.406	0.330	0.149	1.755	1.956	2.653	4.444	3.306
−1.50	2.059	1.243	0.925	0.458	0.361	0.192	1.909	1.296	2.318	3.947	2.968
−1.40	2.324	1.399	1.004	0.516	0.395	0.235	2.072	0.501	1.891	3.361	2.559
−1.30	2.653	1.562	1.091	0.581	0.433	0.280	2.260	−0.373	1.428	2.795	2.166
−1.20	3.022	1.725	1.175	0.649	0.474	0.324	2.476	−1.120	1.041	2.411	1.910
−1.10	3.394	1.857	1.245	0.709	0.515	0.363	2.701	−1.599	0.785	2.199	1.784
−1.00	3.751	1.957	1.296	0.757	0.553	0.397	2.925	−1.834	0.641	2.155	1.756
−0.90	4.110	2.033	1.322	0.795	0.594	0.424	3.117	−2.035	0.508	2.199	1.763
−0.80	4.468	2.102	1.340	0.836	0.638	0.455	3.278	−2.223	0.384	2.280	1.794
−0.70	4.802	2.194	1.405	0.899	0.680	0.499	3.528	−2.273	0.308	2.318	1.822
−0.60	5.116	2.284	1.476	0.962	0.729	0.542	3.790	−2.324	0.231	2.357	1.842
−0.50	5.416	2.377	1.556	1.029	0.782	0.586	4.061	−2.400	0.136	2.376	1.846
−0.40	5.712	2.468	1.635	1.094	0.838	0.629	4.362	−2.445	0.041	2.443	1.858
−0.30	5.978	2.568	1.722	1.165	0.901	0.674	4.680	−2.539	−0.072	2.441	1.853
−0.20	6.224	2.673	1.816	1.237	0.966	0.719	5.031	−2.645	−0.193	2.396	1.841
−0.10	6.460	2.788	1.925	1.315	1.031	0.765	5.392	−2.789	−0.319	2.289	1.816
0.00	6.677	2.913	2.049	1.400	1.098	0.812	5.760	−2.995	−0.462	2.088	1.767
0.10	6.894	3.041	2.198	1.494	1.154	0.857	6.127	−3.209	−0.605	1.843	1.701
0.20	7.111	3.190	2.378	1.610	1.217	0.911	6.505	−3.488	−0.767	1.523	1.617
0.30	7.330	3.364	2.599	1.756	1.292	0.980	6.918	−3.864	−0.960	1.088	1.499

Note. The entire data of Table 6 are available at http://web.yonsei.ac.kr/cosmic/data/YEPS.htm.

Table 7
Input Parameters of CMD Model

Parameters	47 Tuc	NGC 6284	M67
Initial mass function	Salpeter ($x = 1.35$)	Salpeter ($x = 1.35$)	Salpeter ($x = 1.35$)
α-element enhancement, [α/Fe]	0.3	0.3	0.3
HB mass dispersion, $\sigma_M(M_\odot)$	0.015	0.015	0.015
Reimers (1977)'s mass-loss efficiency parameter, η	0.63	0.63	0.63
Distance modulus, $(V - M_V)$ (mag)	13.35	16.70	9.95
Galactic reddening, $E(B - V)$ (mag)	0.01	0.32	0.04
Metal abundance, [Fe/H]	−0.73	−1.50	0.00
Absolute age, t (Gyr)	11.9	13.1	3.5

the model with [α/Fe] $\simeq$ 0.3 (Figure 17). Since Ca4455 is insensitive to the variation of any elements studied in K05, the effect of [α/Fe] shown in Figure 17 comes solely from the variation of Fe due to the increased [α/Fe] at a given Z. This explains why Ca4455 shows a different response compared to Ca4227 even though we treat Ca as a member of the enhanced α-element group (Table 2).

11. G4300. The YEPS model with enhanced α-elements ([α/Fe] = 0.15) for the G4300 shows little offset from the observations (Figure 12). Rather, GCs in the MW and M31 closely follow the model with [α/Fe] = 0.0 (Figure 17). Given that the other lines agree with the observations, our G4300 model seems too sensitive to [α/Fe].
12. $C_2$4668. The YEPS model for the $C_2$4668 index offsets from the observations (Figure 12). The model with enhanced [α/Fe] (Figure 17) shows great sensitivity to [α/Fe]. $C_2$4668 is a measurement of the C abundance and is insensitive to all other α-elements. Because the YEPS model with enhanced [α/Fe] used a fixed C abundance, the strong sensitivity to the α-elements enhancement in Figure 17 comes mainly from the [Fe/H] variation due to the α-element contents at a given Z.
13. NaD. The YEPS model for NaD index is weaker than the observations. Part of the reason for this discrepancy is Na absorption by the interstellar medium (TMB03). As suggested by Coelho et al. (2011), a more realistic model with an increased Na abundance caused by the observed CNONa anticorrelation in the second-generation population would increase the strength of NaD. The Na sensitivity of NaD plays an important role in the α-element-enhanced model by decreasing the strengths of NaD at given Mg b (Figure 17).

Based on the comparison shown in Figures 8–17, we identify several Lick indices that are most appropriate for the estimation of metallicity, age, and α-element enhancement of stellar populations. (1) For determination of iron abundance, Fe4383, Fe4531, Fe5015, Fe5270, and Fe5335 are recommended; (2) for age dating, Balmer indices such as Hβ, Hγ_A, Hγ_F, Hδ_A, and Hδ_F are recommended; and (3) for measuring α-element enhancement, Mg_1, Mg_2, and Mg b are recommended.

4. DISCUSSION

4.1. *Estimation of Age and Metallicity with YEPS*

In this section, we discuss how the effects of HB stars and α-element enhancement in the model are combined to affect the age and metallicity estimation of SSPs. To this aim, we select three typical MWGC, 47 Tucanae (NGC 104), NGC 6284, and M67 (NGC 2682), representing old metal-rich, old metal-poor, and young metal-rich GC populations, respectively. These clusters have well-studied CMDs and show no strong evidence of multiple stellar populations reported by recent studies (Lee et al. 1999; Layden & Sarajedini 1997; Lee et al. 2009c; Han et al. 2009; Ferraro et al. 2009; Piotto et al. 2007; Moretti et al. 2009).

Figure 18 displays the observed and synthetic CMDs for 47 Tuc, NGC 6284, and M67. The free parameters used to match the synthetic CMDs with the observed ones are age and metallicity. To simulate observational errors in our model, we also carried out Monte Carlo simulations based on actual observational uncertainties. The best-fit parameters of each model are summarized in Table 7.

The left column of Figure 19 compares the absorption indices of the observations and models for typical GCs in the MW. Since the YEPS models without HB stars generate very similar results to other models with red clump single-mass HB (Lee et al. 2000), we present the YEPS model with and without HB stars in Figure 19 (1) to highlight the effect of HB and (2) to compare our model with other models with red clump single-mass HBs. The top panel shows that the Hβ indices of the GCs are reproduced better by the model with the HB effect, and the ages based on the absorption lines are in better agreement with the ages (Table 4) derived from synthetic CMDs in Figure 18. In particular, the systematic variation of HB morphologies with respect to metallicity and age is essential to explain the enhanced Hβ strength of NGC 6284—an old, metal-poor system with well-developed blue HB stars. The age of NGC 6284 would be estimated to be 8–9 Gyr without the HB effect, which is inconsistent with its derived age (13.1 Gyr) from the MSTO and the HB morphology in Figure 18. On the other hand, the absorption strengths of 47 Tuc and M67 show reasonable agreement with the YEPS models for 12 Gyr (solid cyan lines) and 3.5 Gyr (between the solid red and orange lines) GCs, respectively. The models for both metal-rich and young clusters possess red HB stars. For a 3 Gyr model GC, the red HB reduces Hβ by 0.2 Å, which corresponds to ∼1 Gyr. Therefore, in order to derive the accurate ages of stellar populations based on the EPS model prediction of Balmer strengths, one should check first whether the EPS model has well-calibrated HBs for both blue HBs (e.g., NGC 6284) and red HBs (e.g., 47 Tuc and M67).

The right column of Figure 19 is similar to the top panel of the left column, but shows the age dating of M31 GCs (Beasley et al. 2004). In these panels, based on the α-element enhancement of GCs in M31 (Puzia et al. 2005), we have used the model of [α/Fe] = 0.15 for comparison. The metal-poor GCs in M31 exhibit stronger Hβ by ∼1 Å than the metal-rich counterparts. When the effect of HBs is not considered, the upper panel of the right column shows that the models give ages ∼5 Gyr younger for the metal-poor GCs compared to the metal-rich GCs in M31. With the general trend of age–metallicity relation in mind, it would be difficult to interpret that the mean age of metal-poor

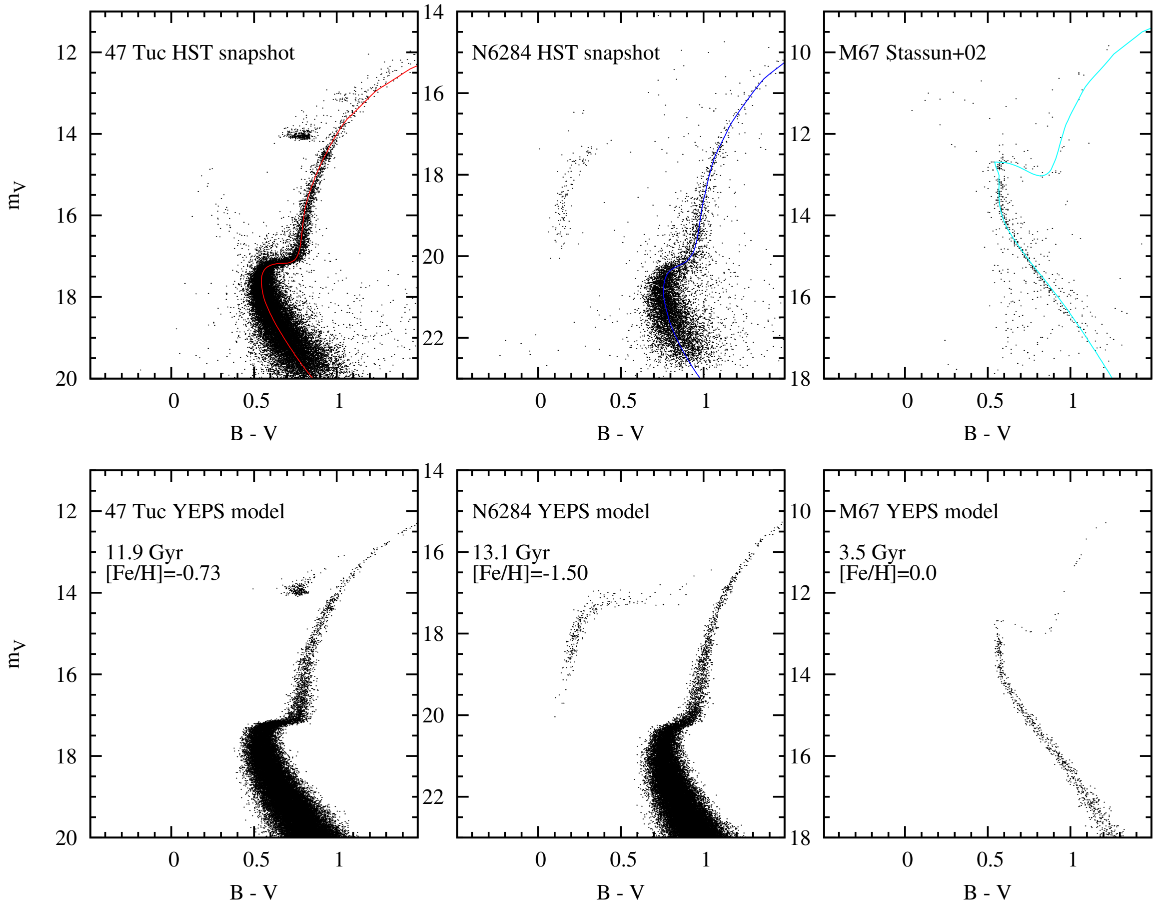

Figure 18. Comparison of the observed 47 Tuc, NGC 6284 (Piotto et al. 2002), and M67 (Stassun et al. 2002) with the synthetic CMD models (bottom panels). The observed CMDs are displayed with matched Y^2-isochrones.

GCs is younger than that of metal-rich GCs. By contrast, the lower panel shows that the systematically enhanced Balmer indices of the metal-poor M31 GCs are well reproduced by our single age, 12 Gyr model GCs with HB stars. Indeed, Perina et al. (2009) directly detected well-developed blue HB stars in the metal-poor GCs in M31 (e.g., B010, B220, B224, and B366) based on the *HST*/ACS CMDs.

In the left column of Figure 19, the middle and bottom panels highlight the effects of HBs and α-element enhancement on the metallicity determination of SSPs. The effects of α-elements and HB stars go in the opposite direction of absorption strengths of Mg *b* for given [Fe/H]'s; the inclusion of blue HB stars decreases indices, whereas the enhancement of α-elements increases indices. While the HBs exert only a marginal effect on determining [Fe/H], the α-elements have a marked effect. For instance, the effect of enhanced α-elements ($[\alpha/\mathrm{Fe}] = 0.3$) on Mg *b* is about 10 times greater than that of HBs when the age and [Fe/H] are assumed to be 12 Gyr and 0.0 dex, respectively. Note that the model line of Mg *b* for 12 Gyr GCs with $[\alpha/\mathrm{Fe}] = 0.3$ is almost identical to that for 4 Gyr GCs with $[\alpha/\mathrm{Fe}] = 0.0$ due to a strong sensitivity of the Mg *b* to the α-elements. In order to determine an accurate $[\alpha/\mathrm{Fe}]$, therefore, the age dating and the metallicity determination of SSPs should be carried out at the same time. The $\langle \mathrm{Fe} \rangle$ index, on the other hand, is less sensitive to $[\alpha/\mathrm{Fe}]$ than Mg *b*, which makes $\langle \mathrm{Fe} \rangle$ a more accurate [Fe/H] indicator for SSPs than other indices sensitive to $[\alpha/\mathrm{Fe}]$ (e.g., Mg *b* and Mg_2).

Since the age dating with Balmer indices is usually applied to the samples of elliptical galaxies (e.g., Trager et al. 2000; Caldwell et al. 2003; Thomas et al. 2005; Nelan et al. 2005; Trager et al. 2008; Graves et al. 2009), the effect of HB stars is also important for composite stellar populations. The effect of HB stars on the integrated observables of giant elliptical galaxies should be limited because their mean metallicities are as high as $[\mathrm{Z/H}] > 0.0$, for which hot HB stars are rare. But the metallicity spread of ellipticals, nevertheless, allows them to have a certain fraction of low-metallicity stars and thus hot HB stars accordingly (Park & Lee 1997; Chung et al. 2011). Moreover, the effect of hot HB stars in dwarf elliptical galaxies is more important because the metallicity of dwarf ellipticals is generally lower than that of giant ellipticals. In the context of galaxy downsizing (e.g., Cowie et al. 1996), the age dating of giant and dwarf elliptical galaxies with well-calibrated HB models is a crucial issue for determining the formation history of elliptical galaxies. We will fully discuss this issue in a forthcoming paper (C. Chung et al. 2013, in preparation).

4.2. *Distributions of Absorption Indices in Extragalactic GCs*

Ever since the recognition of bimodal broadband color distributions of GCs in massive early-type galaxies (Zepf & Ashman 1993; Geisler et al. 1996; Forbes et al. 1997; Gebhardt 1999; Kundu 2001; Larsen et al. 2001; Jordan et al. 2002; Puzia et al. 2004; West et al. 2004; Strader et al. 2006; Peng et al. 2006; Harris et al. 2006; Jordán et al. 2009; Liu et al. 2011), the phenomenon has been interpreted as the presence of two GC subsystems within individual galaxies. Three major ideas have been put forward to explain it, including the merger model

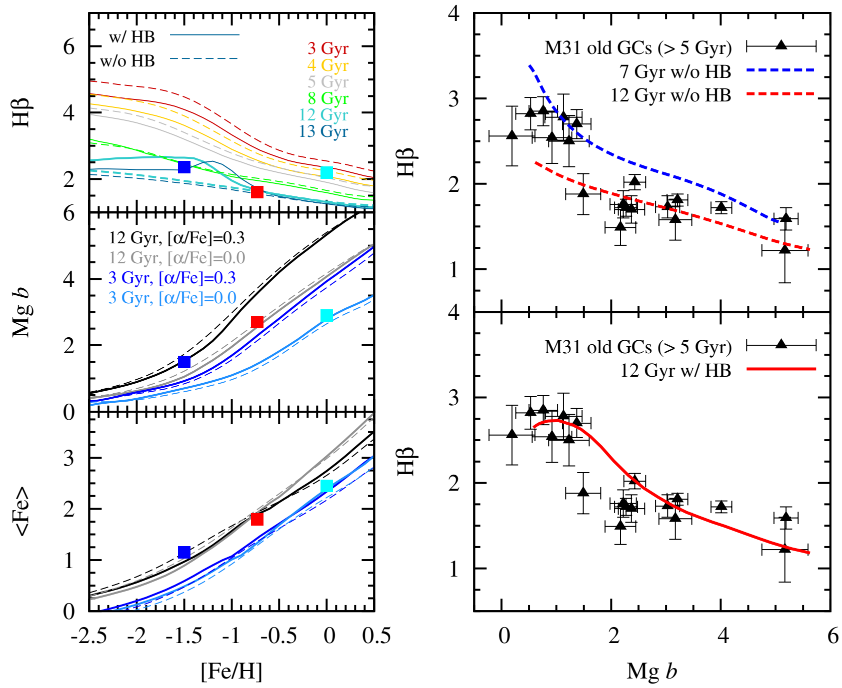

Figure 19. Comparison of the YEPS model with the observed absorption indices of NGC 6284, 47 Tuc (Schiavon et al. 2005, 2012), and M67 (Schiavon 2007), as well as GCs in M31 (Beasley et al. 2004). The blue, red, and cyan squares in the left panels are observed as the integrated absorption indices of NGC 6284, 47 Tuc, and M67. The solid and long dashed lines in all the panels are models with and without HB stars. The red, orange, gray, green, turquoise, and blue lines in the left top panel represent the Hβ models for the ages of 3, 4, 5, 8, 12 and 13 Gyr with $[\alpha/\mathrm{Fe}] = 0.3$. The gray and black lines in the middle and bottom panels on the left side are models for $[\alpha/\mathrm{Fe}] = 0.0$ and 0.3 at the age of 12 Gyr. The light blue and blue lines in the same panels are models for $[\alpha/\mathrm{Fe}] = 0.0$ and 0.3 at the age of 3 Gyr. In the right panels, the effect of HB stars on age dating with the Hβ is displayed with M31 GCs (Beasley et al. 2004). The model lines in the right panels are for $[\alpha/\mathrm{Fe}] = 0.15$.

(e.g., Ashman & Zepf 1992), the in situ (e.g., Forbes et al. 1998), and accretion (e.g., Cote et al. 1998) scenarios.

More recently, however, Yoon et al. (2006) and Yoon et al. (2011a, 2011b) suggested an alternative explanation for the GC color bimodality that does not necessarily invoke two GC subpopulations. Yoon et al. show that the theoretical metallicity–color relations are inflected, and that such relations can generate bimodal color distributions from broad metallicity spreads, even if they are unimodal. The Yoon et al. (2006) model of GC colors indicates that the HB effect is the most important for the inflection on the metallicity–color relations. HBs also have a strong effect on the absorption index versus metallicity relations (IMRs), and thus one can put the Yoon et al. explanation to the test by examining the metallicity–index nonlinearity and the resulting index distributions.

4.2.1. Conversions from Metallicity Spreads to Index Distributions

Figure 20 shows the conversion from metallicity spreads to index distributions via IMRs. Three different ages are selected that show little (5 Gyr) and significant (12 and 13 Gyr) inflection on the IMRs. We assume the underlying metallicity distribution functions (MDFs) of 10^6 model GCs to be box shaped and perform the Monte Carlo simulations for index distributions. The simple MDFs should allow us to see the pure effect of the IMR projection. The indices of each model GC are calculated from its [Fe/H] value via corresponding IMRs and then typical errors estimated from observations from Beasley et al. (2004) are randomly added. Our simulations with the non-inflected IMRs do not produce bimodal index distributions. For example, Fe4531 and Fe5782 of the 5 Gyr models are trapezoid shaped. In many cases, the index histograms have a sharp peak with a long tail as the IMRs are broken roughly into parts—the metal-poor, steep section and the metal-rich, shallow section. On the other hand, the index distributions produced by the highly inflected IMRs clearly show bimodality. For example, the IMRs for G4300, Hβ, H$\gamma_{A,F}$, and H$\delta_{A,F}$ of the old GCs have a very shallow slope at $[\mathrm{Fe/H}] \simeq -1.0$ between two steeper slopes. The inflection brings about a dip on the index distributions by projecting equidistant metallicity intervals onto larger index intervals.

Figure 21 repeats a similar experiment but uses Gaussian MDFs. We test for the two Gaussian MDFs of $\langle[\mathrm{Fe/H}]\rangle = -1.0$ and -0.7 with the same dispersion of $\sigma_{[\mathrm{Fe/H}]} = 0.55$. In this simulation, we also have applied 10^6 model GCs for the given Gaussian MDFs. Even with Gaussian MDFs, the projected index distributions are double-peaked for G4300, Hβ, H$\gamma_{A,F}$, and H$\delta_{A,F}$ of 12 Gyr model GCs. When an MDF with $\langle[\mathrm{Fe/H}]\rangle = -1.0$ is used, for example, the KMM algorithm (Ashman et al. 1994) strongly prefers two peaks for these histograms with p-value $\simeq 0.0$. For the projected Hβ distribution under the assumption of the 12 Gyr model, the two peaks are located at 1.681 Å and 2.535 Å with a number fraction of 48.6% and 51.4%, respectively.

It has been claimed that the bimodal distributions of metal-line indices (e.g., Mg b and [MgFe]′) of GCs in early-type galaxies are evidence that GCs have two subsystems with different metallicities (Cohen et al. 1998, 2003; Strader et al. 2007; Woodley et al. 2010). Interestingly, however, even with a unimodal MDF, the index distribution of Mg b, frequently used as a metallicity indicator, also shows a bimodal index distribution that is consistent with the observations. Our KMM test for the projected Mg b distribution of the 12 and 13 Gyr models supports bimodal distributions with a p-value of 0.0. The test implies that the HBs exert an appreciable effect not only

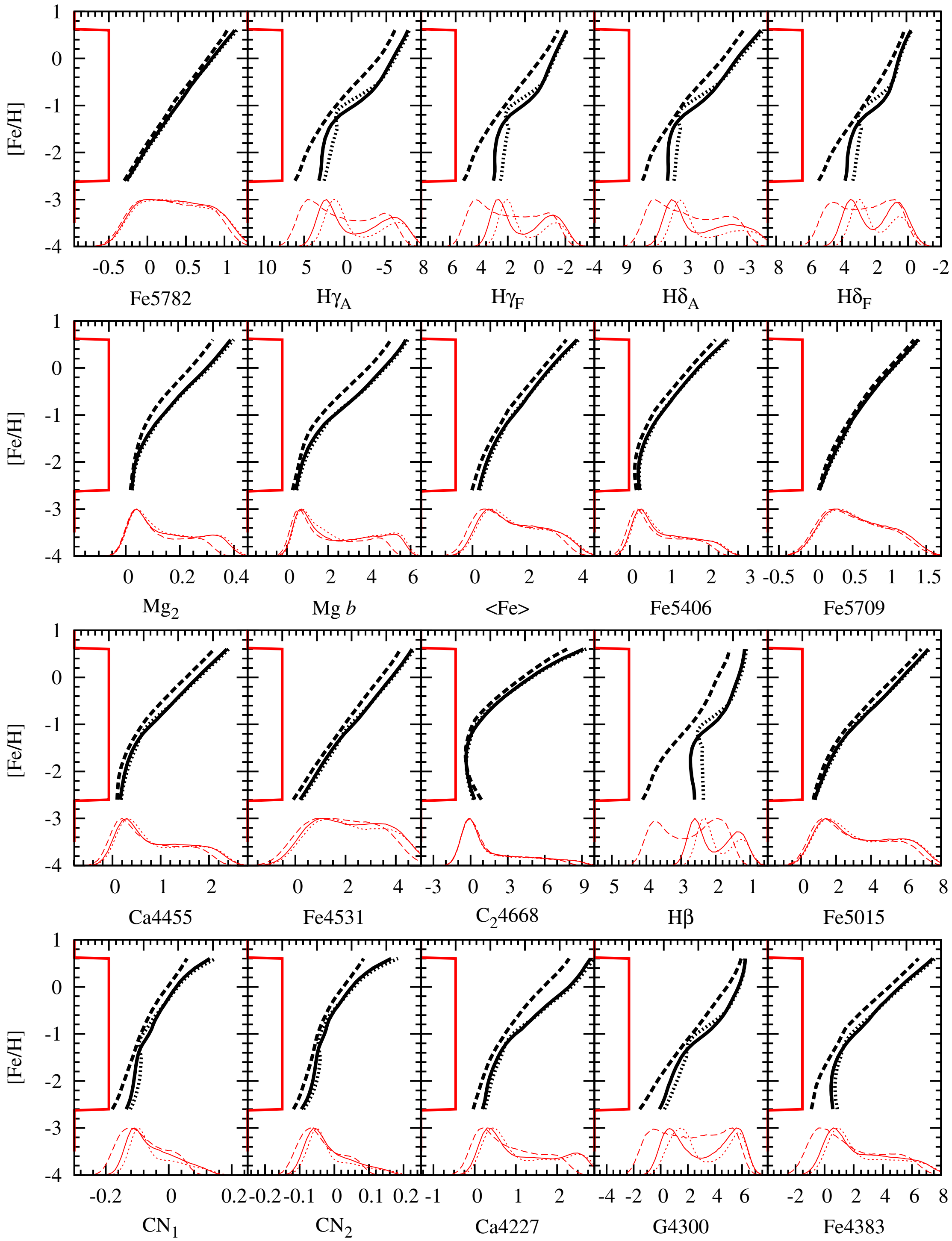

Figure 20. Test of the projection effect with the box-shaped metallicity distribution function (MDF) on various Lick absorption indices. The box-shaped MDFs of 10^6 model GCs are shown along the y-axis. The black dashed, solid, and dotted lines in each plot indicate 5, 12, and 13 Gyr models with $[\alpha/\mathrm{Fe}] = 0.15$ for given Lick indices. The red dashed, solid, and dotted lines in the bottom of each plot show the result of the box-MDF projection to various Lick absorption indices. The absorption index distributions of each line type correspond to the projection of the models with the same line type.

on the Balmer lines but also on the metallicity-sensitive lines. Without assuming two subpopulations in GCs, the projection effect can reproduce the observed bimodal Mg *b* histograms.

4.2.2. Absorption Index Distributions of M31 Globular Clusters

In order to compare the observational index distributions with the simulated ones, we choose M31, the nearest large galaxy, which has spectroscopic surveys of a great number of GCs with reasonably small observation errors. M31 GCs (Beasley et al. 2004) have 18% and 33% smaller errors respectively in Hβ and $\langle\mathrm{Fe}\rangle$ at given absolute magnitudes compared to the M87 GC spectroscopy with Subaru (S. Kim et al. 2013, in preparation). We excluded young cluster candidates in Beasley et al. (2004) to avoid young cluster contaminations in the MDF (see blue triangles in Figure 8–12).

Figure 22 shows the index–index diagrams for $\langle\mathrm{Fe}\rangle$ and Balmer indices. The observed index distributions of M31

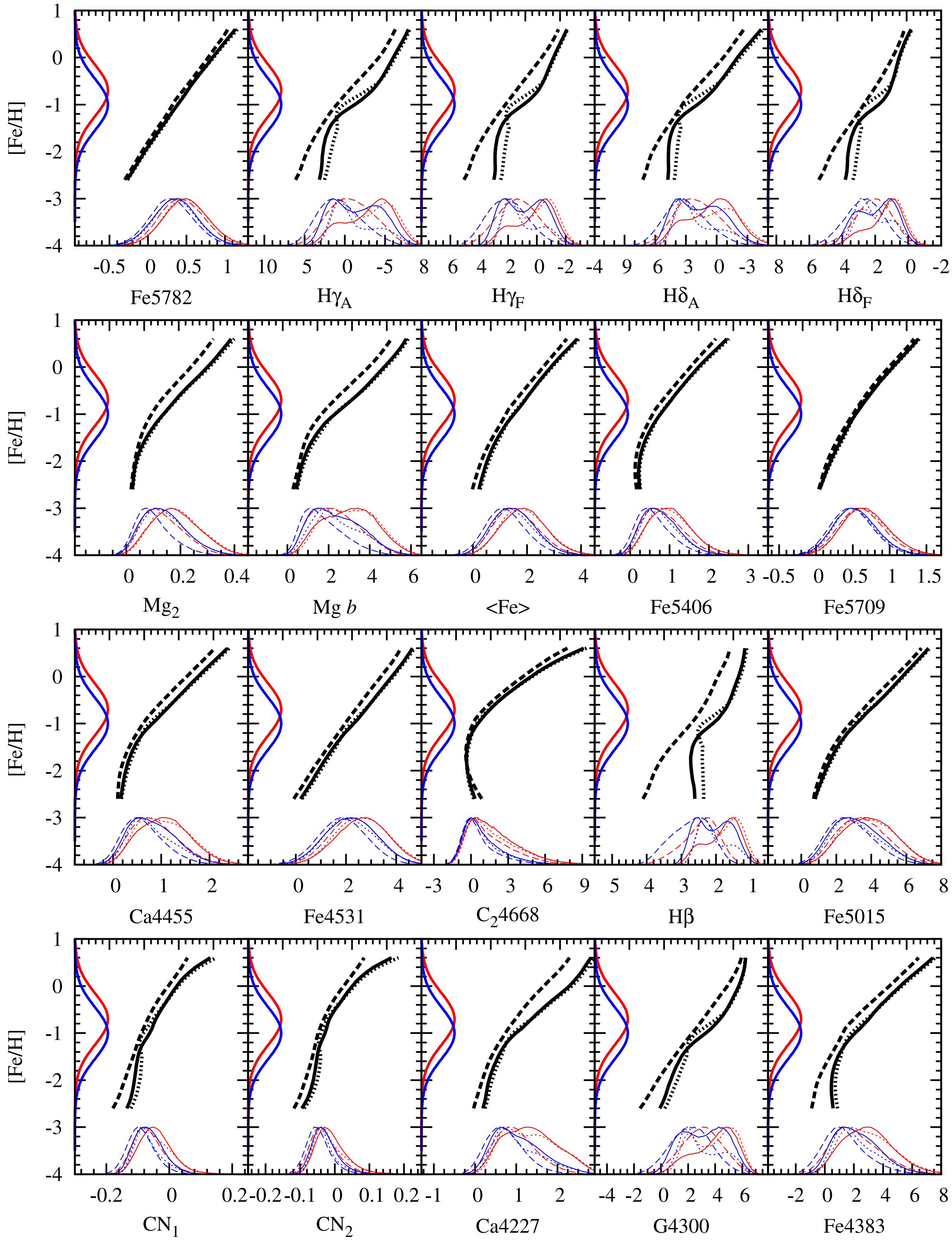

Figure 21. Same as Figure 20 but for the projection tests with the single Gaussian MDFs of $\langle[\mathrm{Fe/H}]\rangle = -0.7$ (red) and -1.0 (blue) on various Lick absorption indices. The 10^6 model GCs with single Gaussian MDFs are projected on various absorption indices via IMRs of the YEPS model.

GCs and the projection simulations based on the YEPS and TMB03 IMRs are shown as histograms along the *y*- and *x*-axes, respectively. We, again, make a simple assumption of Gaussian MDFs with $\langle[\mathrm{Fe/H}]\rangle = -1.0$ and $\sigma_{[\mathrm{Fe/H}]} = 0.55$. As explained in detail in Section 4.2.1, the principle of the MDF projection with IMRs is to transfer SSPs from the metallicity space to the index space. The red circles with uniform metallicity intervals ($\Delta[\mathrm{Fe/H}] \simeq 0.3$) on the YEPS IMRs in the bottom panel show this principle of projection. All Balmer indices show large index space between [Fe/H] $= -1.1$ to -0.5, and the corresponding index distributions also show relatively low number frequencies. However, the $\langle\mathrm{Fe}\rangle$ index, which keeps relatively constant index intervals at fixed [Fe/H] intervals, does not show a significant change in the projected distribution. As a result, the projection

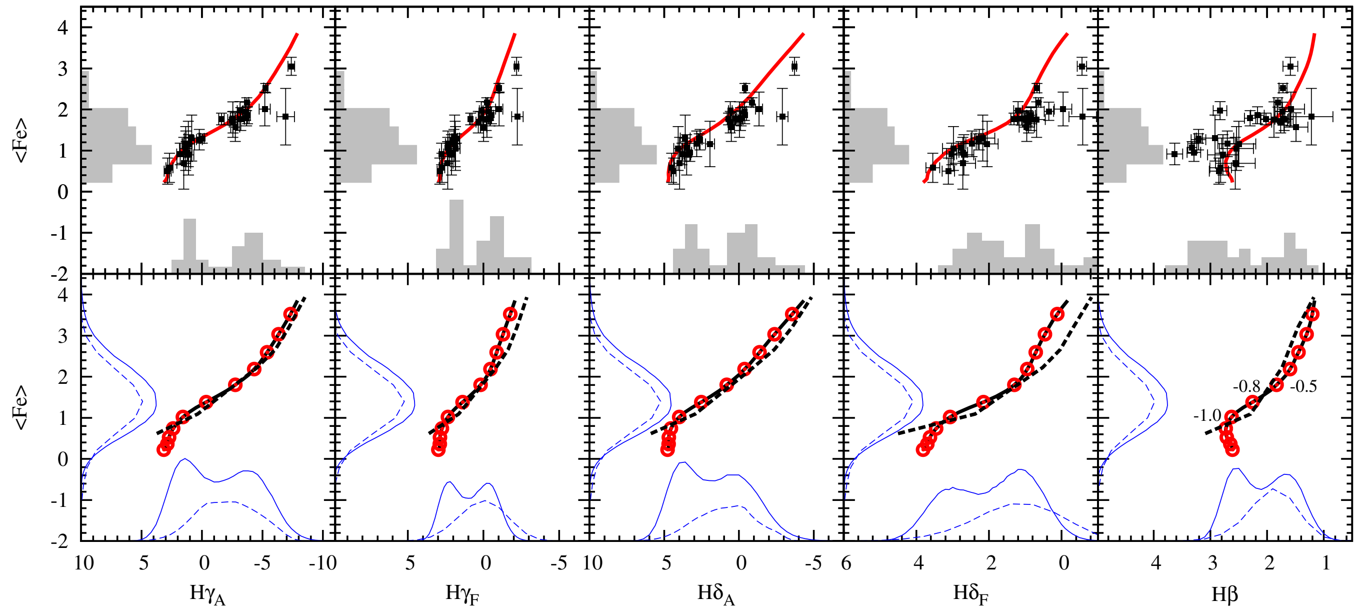

Figure 22. Comparison between the index distributions of M31 GCs and simulated index distributions. The upper panels are observed histograms of M31 GCs in Hβ, H$\gamma_{A,F}$, H$\delta_{A,F}$, and ⟨Fe⟩, and the YEPS models (red lines) for each index are overlaid with GCs in M31. The lower panels are simulated index distributions with the YEPS and TMB03 models. The black solid and dashed lines represent the YEPS and TMB03 model for [α/Fe] = 0.15, respectively. The blue solid and dashed lines are simulated index distributions based on the YEPS and TMB03 model, respectively. The red circles on the solid lines indicate metallicities from [Fe/H] = −2.6 to −0.5 with a fixed interval Δ[Fe/H] = 0.3. The three values of [Fe/H] = −1.0, −0.8, and −0.5 are indicated in the YEPS model for Hβ.

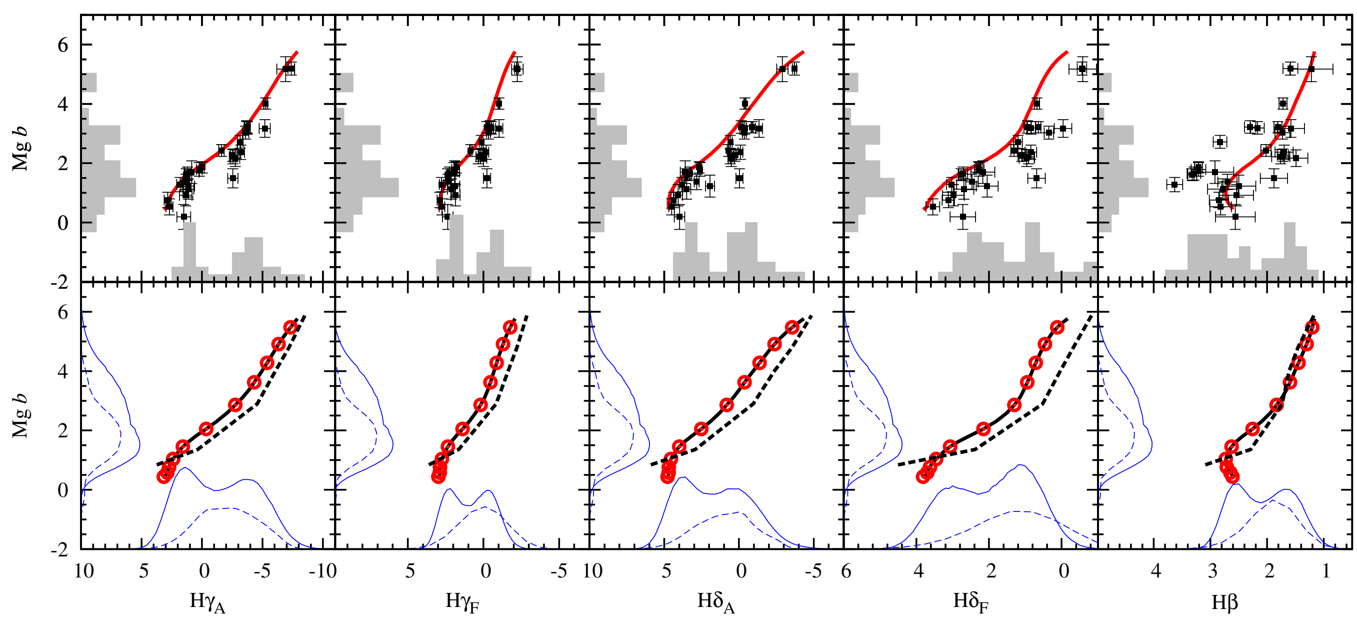

Figure 23. Same as Figure 22 but for Mg *b* distributions.

simulation with the YEPS model reproduces the unimodal ⟨Fe⟩ and bimodal Balmer line distributions at the same time using a single Gaussian MDF. We stress that if the observational errors are small enough, then the ⟨Fe⟩ distributions can also show a weak bimodal feature. Indeed, the recent observation of GCs in M31 by Caldwell et al. (2011) shows a weak bimodality in the distribution of ⟨Fe⟩ (Kim et al. 2012). The TMB03 model, on the other hand, gives almost straight IMRs and does not reproduce the observed distributions of the ⟨Fe⟩ and Balmer indices, simultaneously. No matter how small the errors are, the single Gaussian MDF projection based on the models without systematic HB effect cannot reproduce the observed distributions for both ⟨Fe⟩ and Balmer indices.

Figure 23 shows the index–index diagrams for Mg *b* and Balmer indices. The observed and simulated Mg *b* and Balmer distributions are displayed along the *y*- and *x*-axes, respectively. As discussed in Section 4.2.1, Mg *b* is fairly affected by blue HBs, and thus the distribution of Mg *b* shows weak bimodality. Many other observations of GCs in early type galaxies also show similar results and the bimodal Mg *b* distributions are often interpreted as evidence of the bimodal GC MDFs (Cohen et al. 1998, 2003; Strader et al. 2007; Woodley et al. 2010). The comparison of the YEPS model to M31 GCs demonstrates that the HB effect on Mg *b* is certainly non-negligible. Greater caution, therefore, is required in deriving GC metallicity directly from Mg *b*.

The spectroscopic line indices, with more detailed probes of stellar populations than broadband colors, contain abundant information on the structure of GC systems. Our simulations targeting the old GCs in M31 suggest that two distinct groups found in Balmer and Mg *b* indices could be due simply to inflected, nonlinear IMRs. The result favors a unimodal [Fe/H] distribution of M31 old GCs, in line with the GC structure of extragalactic GC systems suggested by Yoon et al. (2006, 2011a, 2011b). Absorption indices are generally subject to larger observational uncertainties, and spectroscopic samples are still small compared to photometric samples with broadband colors. More precise spectroscopic observations of a greater number of extragalactic GCs by next-generation telescope projects, such as the Giant Magellan Telescope, Thirty Meter Telescope (TMT), and European Extremely Large Telescope, are highly anticipated in this regard.

5. SUMMARY

We have presented an updated and blown-up version of the YEPS model for spectroscopic absorption indices of SSPs. The characteristics of the YEPS and its applications are summarized as follows.

1. YEPS includes detailed HB models, which reproduce the observed HB morphology of Milky Way GCs and vary with respect to metallicity, age, and α-element enhancement.
2. YEPS incorporates the α-element variation by using the Y^2 stellar library with enhanced α-elements and the response functions of α-elements by K05.
3. YEPS is in good agreement with other EPS models, except for the indices sensitive to hot stars (CN_1, CN_2, G4300, Hβ, Hγ, and Hδ).
4. YEPS reproduces well the observed absorption features of GCs in the MW and M31, including the strengthened Balmer absorptions by the effect of blue HBs.
5. When the observed variation of HB morphology with metallicity in the MWGCs is included in the models, Balmer indices of SSPs do not monotonically decrease with increasing metallicity at a given age because of blue HB stars in the metal-poor regime. Therefore, the age dating of old stellar systems based on Balmer indices suffers from age degeneracy in the metal-poor regime.
6. The contribution of HBs to absorption strengths is not limited to Balmer indices but influences the indices pertinent to iron and α-elements. As a consequence, the most IMRs of YEPS are inflected and nonlinear.
7. We have simulated, for the first time, the index distributions of GCs using YEPS IMRs. The distributions of Balmer and Mg *b* indices constructed under the unimodal MDF assumption show clear bimodality, which can be viewed as a close analogy to the well-known bimodality found in the broadband color distributions of extragalactic GC systems.

We thank the referee for a number of helpful suggestions. S.-J.Y. and Y.-W.L. acknowledge support from the National Research Foundation of Korea to the Center for Galaxy Evolution Research. S.-J.Y. also acknowledges support from the Basic Science Research Program (No. 2011-0027247) through a National Research Foundation (NRF) of Korea grant funded by the Ministry of Education, Science and Technology (MEST), and support by the Korea Astronomy and Space Science Institute (KASI) Research Fund 2011 and 2012. S.-J.Y. thanks Daniel Fabricant, Charles Alcock, Jay Strader, Nelson Caldwell, Dong-Woo Kim, and Jae-Sub Hong for their hospitality during his stay at the Harvard-Smithsonian Center for Astrophysics in 2011–2012. This work was partially supported by the KASI-Yonsei Joint Research Program (2011–2012) for the Frontiers of Astronomy and Space Science.

REFERENCES

Arimoto, N., & Yoshii, Y. 1987, A&A, 173, 23
Ashman, K. M., Bird, C. M., & Zepf, S. E. 1994, AJ, 108, 2348
Ashman, K. M., & Zepf, S. E. 1992, ApJ, 384, 50
Beasley, M. A., Brodie, J. P., Strader, J., et al. 2004, AJ, 128, 1623
Bono, G., Caputo, F., Cassisi, S., Castellani, V., & Marconi, M. 1997, ApJ, 489, 822
Bressan, A., Chiosi, C., & Fagotto, F. 1994, ApJS, 94, 63
Bruzual, A. G. 1983, ApJ, 273, 105
Bruzual, A. G., & Charlot, S. 1993, ApJ, 405, 538
Bruzual, G., & Charlot, S. 2003, MNRAS, 344, 1000
Burstein, D., Faber, S. M., Gaskell, C. M., & Krumm, N. 1984, ApJ, 287, 586
Buzzoni, A. 1989, ApJS, 71, 817
Buzzoni, A., Gariboldi, G., & Mantegazza, L. 1992, AJ, 103, 1814
Buzzoni, A., Mantegazza, L., & Gariboldi, G. 1994, AJ, 107, 513
Caldwell, N., Rose, J. A., & Concannon, K. D. 2003, AJ, 125, 2891
Caldwell, N., Schiavon, R., Morrison, H., Rose, J. A., & Harding, P. 2011, AJ, 141, 61
Carretta, E., Bragaglia, A., Gratton, R. G., et al. 2009, A&A, 505, 117
Carretta, E., Gratton, R. G., Lucatello, S., Bragaglia, A., & Bonifacio, P. 2005, A&A, 433, 597
Cassisi, S., Castellani, M., & Castellani, V. 1997, A&A, 317, 108
Cassisi, S., Salaris, M., Castelli, F., & Pietrinferni, A. 2004, ApJ, 616, 498
Cervantes, J. L., & Vazdekis, A. 2009, MNRAS, 392, 691
Chaboyer, B., Demarque, P., Kernan, P. J., & Krauss, L. M. 1998, ApJ, 494, 96
Cho, J., Sharples, R. M., Blakeslee, J. P., et al. 2012, MNRAS, 422, 3591
Choi, Y., Goto, T., & Yoon, S.-J. 2009, MNRAS, 395, 637
Chung, C., Yoon, S.-J., & Lee, Y.-W. 2011, ApJL, 740, 45
Coelho, P., Percival, S. M., & Salaris, M. 2011, ApJ, 734, 72
Cohen, J. G., Blakeslee, J. P., & Côté, P. 2003, ApJ, 592, 866
Cohen, J. G., Blakeslee, J. P., & Ryzhov, A. 1998, ApJ, 496, 808
Conroy, C., & Gunn, J. E. 2010, ApJ, 712, 833
Cote, P., Marzke, R. O., & West, M. J. 1998, ApJ, 501, 554
Cowie, L. L., Songaila, A., Hu, E. M., & Cohen, J. G. 1996, AJ, 112, 839
Diaz, A. I., Terlevich, E., & Terlevich, R. 1989, MNRAS, 239, 325
Dotter, A., Sarajedini, A., Anderson, J., et al. 2010, ApJ, 708, 698
Faber, S. M. 1973, ApJ, 179, 731
Faber, S. M., Friel, E. D., Burstein, D., & Gaskell, C. M. 1985, ApJS, 57, 711
Ferraro, F. R., Dalessandro, E., Mucciarelli, A., et al. 2009, Natur, 462, 483
Fioc, M., & Rocca-Volmerange, B. 1997, A&A, 326, 950
Forbes, D. A., Brodie, J. P., & Huchra, J. 1997, AJ, 113, 887
Forbes, D. A., Grillmair, C. J., Williger, G. M., Elson, R. A. W., & Brodie, J. P. 1998, MNRAS, 293, 325
Fritze-Von Alvensleben, U. A., & Gerhard, O. E. 1994, A&A, 285, 751
Gebhardt, K., & Kissler-Patig, M. 1999, AJ, 118, 1526
Geisler, D., Lee, M. G., & Kim, E. 1996, AJ, 111, 1529
Gratton, R., Sneden, C., & Carretta, E. 2004, ARA&A, 42, 385
Gratton, R. G., Pecci, F. F., Carretta, E., et al. 1997, ApJ, 491, 749
Graves, G. J., Faber, S. M., & Schiavon, R. P. 2009, ApJ, 693, 486
Grevesse, N., & Noels, A. 1993, in Origin and Evolution of the Elements, ed. N. Prantzos, E. Vangioni-Flam, & M. Casse (Cambridge: Cambridge Univ. Press), 15
Guiderdoni, B., & Rocca-Volmerange, B. 1987, A&A, 186, 1
Han, S.-I., Lee, Y.-W., Joo, S.-J., et al. 2009, ApJL, 707, 190
Harris, W. E., Whitmore, B. C., Karakla, D., et al. 2006, ApJ, 636, 90
Johansson, J., Thomas, D., Maraston, C., et al. 2010, MNRAS, 406, 165
Jones, L. A. 1999, PhD thesis, Univ. North Carolina
Jones, L. A., & Worthey, G. 1995, ApJL, 446, 31
Jordán, A., Peng, E. W., Blakeslee, J. P., et al. 2009, ApJS, 180, 54
Jordan, A. S., Cote, P., West, M. J., & Marzke, R. O. 2002, ApJL, 576, 113
Kaviraj, S., Ferreras, I., Yoon, S.-J., & Yi, S. K. 2005, A&A, 439, 913
Kaviraj, S., Schawinski, K., Devriendt, J. E. G., et al. 2007a, ApJS, 173, 619
Kaviraj, S., Sohn, S. T., O'Connell, R. W., et al. 2007b, MNRAS, 377, 987
Kaviraj, S., Rey, S.-C., Rich, R. M., Yoon, S.-J., & Yi, S. K. 2007c, MNRAS, 381, L74
Kim, J.-W., Kang, A., Rhee, J., et al. 2006, A&A, 459, 499
Kim, S., Yoon, S.-J., Chung, C., et al. 2012, ApJ, submitted

Kim, Y.-C., Demarque, P., Yi, S. K., & Alexander, D. R. 2002, ApJS, 143, 499
Korn, A. J., Maraston, C., & Thomas, D. 2005, A&A, 438, 685
Kundu, A., & Whitmore, B. C. 2001, AJ, 121, 2950
Kurucz, R. L. 1992, in IAU Symp. 149, The Stellar Populations of Galaxies, ed. B. Barbuy & A. Renzini (Dordrecht: Kluwer), 225
Larsen, S. S., Brodie, J. P., Huchra, J. P., Forbes, D. A., & Grillmair, C. J. 2001, AJ, 121, 2974
Layden, A. C., & Sarajedini, A. 1997, ApJL, 486, 107
Lee, H.-C., & Worthey, G. 2005, ApJS, 160, 176
Lee, H.-C., Worthey, G., & Blakeslee, J. P. 2010, ApJ, 710, 421
Lee, H.-C., Worthey, G., & Dotter, A. 2009a, AJ, 138, 1442
Lee, H.-C., Worthey, G., Dotter, A., et al. 2009b, ApJ, 694, 902
Lee, H.-C., Yoon, S.-J., & Lee, Y.-W. 2000, AJ, 120, 998
Lee, J.-W., Kang, Y.-W., Lee, J., & Lee, Y.-W. 2009c, Natur, 462, 480
Lee, Y.-W., Demarque, P., & Zinn, R. 1990, ApJ, 350, 155
Lee, Y.-W., Demarque, P., & Zinn, R. 1994, ApJ, 423, 248
Lee, Y.-W., Gim, H. B., & Casetti-Dinescu, D. I. 2007, ApJL, 661, 49
Lee, Y.-W., Joo, J. M., Sohn, Y. J., et al. 1999, Natur, 402, 55
Lee, Y.-W., Joo, S.-J., Han, S.-Il., et al. 2005a, ApJL, 621, 57
Lee, Y.-W., Ree, C. H., Rich, R. M., et al. 2005b, ApJL, 619, 103
Lejeune, T., Cuisinier, F., & Buser, R. 1998, A&AS, 130, 65
Letherer, C., & Heckman, T. 1995, ApJS, 96, 9
Liu, C., Peng, E. W., Jordán, A., et al. 2011, ApJ, 728, 116
Maraston, C. 1998, MNRAS, 300, 872
Maraston, C., Greggio, L., Renzini, A., et al. 2003, A&A, 400, 823
Maraston, C., & Strömbäck, G. 2011, MNRAS, 418, 2785
Marín-Franch, A., Aparicio, A., Piotto, G., et al. 2009, ApJ, 694, 1498
Mendel, J. T., Proctor, R. N., & Forbes, D. A. 2007, MNRAS, 379, 1618
Mieske, S., Hilker, M., Bomans, D. J., et al. 2008, A&A, 489, 1023
Moretti, A., Piotto, G., Arcidiacono, C., et al. 2009, A&A, 493, 539
Munari, U., Sordo, R., Castelli, F., & Zwitter, T. 2005, A&A, 442, 1127
Nelan, J. E., Smith, R. J., Hudson, M. J., et al. 2005, ApJ, 632, 137
Park, J.-H, & Lee, Y.-W. 1997, ApJ, 476, 28
Peng, E. W., Jordán, A., Côté, P., et al. 2006, ApJ, 639, 95
Percival, S. M., & Salaris, M. 2011, MNRAS, 412, 2445
Perina, S., Federici, L., Bellazzini, M., et al. 2009, A&A, 507, 1375
Pietrinferni, A., Cassisi, S., Salaris, M., & Castelli, F. 2004, ApJ, 612, 16
Piotto, G., Bedin, L. R., Anderson, J., et al. 2007, ApJL, 661, 53
Piotto, G., King, I. R., Djorgovski, S. G., et al. 2002, A&A, 391, 945
Pforr, J., Maraston, C., & Tonini, C. 2012, MNRAS, 422, 3285
Pritzl, B. J., Venn, K. A., & Irwin, M. 2005, AJ, 130, 2140
Puzia, T. H., Kissler-Patig, M., Thomas, D., et al. 2004, A&A, 415, 123
Puzia, T. H., Perrett, K. M., & Bridges, T. J. 2005, A&A, 434, 909
Ree, C. H., Lee, Y.-W., Yi, S. K., et al. 2007, ApJS, 173, 607
Reid, I. N. 1997, AJ, 114, 161
Reimers, D. 1977, A&A, 57, 395
Rey, S.-C., Rich, R. M., Lee, Y.-W., et al. 2005, ApJL, 619, 119
Rey, S.-C., Rich, R. M., Sohn, S. T., et al. 2007, ApJS, 173, 643
Rey, S.-C., Sohn, S. T., Beasley, M. A., et al. 2009, ApJL, 700, 11
Rey, S.-C., Yoon, S.-J., Lee, Y.-W., Chaboyer, B., & Sarajedini, A. 2001, AJ, 122, 3219
Rood, R. T. 1973, ApJ, 184, 815
Rose, J. A. 1984, AJ, 89, 1238
Rose, J. A. 1985, AJ, 90, 1927
Salasnich, B., Girardi, L., Weiss, A., & Chiosi, C. 2000, A&A, 361, 1023
Schiavon, R. P. 2007, ApJS, 171, 146
Schiavon, R. P., Caldwell, N., Morrison, H., et al. 2012, AJ, 143, 14
Schiavon, R. P., Rose, J. A., Courteau, S., & MacArthur, L. A. 2005, ApJS, 160, 163
Schulz, J., Fritze-v. Alvensleben, U., Moller, C. S., & Fricke, K. J. 2002, A&A, 392, 1
Spitler, L. R., Forbes, D. A., & Beasley, M. A. 2008, MNRAS, 389, 1150
Stassun, K. G., van den Berg, M., Mathieu, R. D., & Verbunt, F. 2002, A&A, 382, 899
Strader, J., Beasley, M. A., & Brodie, J. P. 2007, AJ, 133, 2015
Strader, J., Brodie, J. P., Spitler, L., & Beasley, M. A. 2006, AJ, 132, 2333
Thomas, D., Johansson, J., & Maraston, C. 2011, MNRAS, 412, 2199
Thomas, D., Maraston, C., & Bender, R. 2003, MNRAS, 339, 897
Thomas, D., Maraston, C., Bender, R., & Mendes de Oliveira, C. 2005, ApJ, 621, 673
Tinsley, B. M. 1972, ApJ, 178, 319
Tinsley, B. M. 1978, ApJ, 222, 14
Trager, S. C., Faber, S. M., & Dressler, A. 2008, MNRAS, 386, 715
Trager, S. C., Faber, S. M., Worthey, G., & Gonzalez, J. J. 2000, AJ, 119, 1645
Tripicco, M. J., & Bell, R. A. 1995, AJ, 110, 3035
VandenBerg, D. A., Swenson, F. J., Rogers, F. J., Iglesias, C. A., & Alexander, D. R. 2000, ApJ, 532, 430
Vazdekis, A. 1999, ApJ, 513, 224
Vazdekis, A., Sánchez-Blázquez, P., Falcón-Barroso, J., et al. 2010, MNRAS, 404, 1639
West, M. J., Cote, P., Marzke, R. O., & Jordan, A. 2004, Natur, 427, 31
Westera, P., Lejeune, T., Buser, R., Cuisinier, F., & Bruzual, G. 2002, A&A, 381, 524
Woodley, K. A., Harris, W. E., Puzia, T. H., et al. 2010, ApJ, 708, 1335
Worthey, G. 1994a, ApJS, 94, 687
Worthey, G. 1994b, ApJS, 95, 107
Worthey, G., & Ottaviani, D. L. 1997, ApJS, 111, 377
Yi, S., Demarque, P., & Oemler, A., Jr. 1997, ApJ, 486, 201
Yoon, S.-J., & Chung, C. 2009, in Globular Clusters–Guides to Galaxies, ed. T. Richtter & S. Larsen (ESO Astrophysics Symposia; Berlin: Springer), 381
Yoon, S.-J., Joo, S.-J., Ree, C. H., et al. 2008, ApJ, 677, 1080
Yoon, S.-J., Kim, H.-S., Sohn, S. T., et al. 2012, ApJ, submitted
Yoon, S.-J., Lee, S.-Y., Blakeslee, J. P., et al. 2011a, ApJ, 743, 150
Yoon, S.-J., & Lee, Y.-W. 2002, Science, 297, 578
Yoon, S.-J., Sohn, S. T., Lee, S.-Y., et al. 2011b, ApJ, 743, 149
Yoon, S.-J., Yi, S. K., & Lee, Y.-W. 2006, Science, 311, 1129
Yoon, S.-J., Yi, S. K., & Lee, Y.-W. 2009, in Globular Clusters–Guides to Galaxies, ed. T. Richtter & S. Larsen (ESO Astrophysics Symposia; Berlin: Springer), 367
Zepf, S. E., & Ashman, K. M. 1993, MNRAS, 264, 611